Regulating the Translocation of DNA through Poly(N-isopropylacrylamide)-Decorated Switchable Nanopores by Cononsolvency Effect

Huaisong Yong, Bastien Molcrette, Marcel Sperling, Fabien Montel, Jens-Uwe Sommer

Regulating the translocation of DNA through poly(N-isopropylacrylamide) decorated switchable nanopores by cononsolvency effect

Huaisong Yong[1,2,*], Bastien Molcrette[3], Marcel Sperling[4], Fabien Montel[3,*], and Jens-Uwe Sommer[1,5,*]

[1]Leibniz-Institut für Polymerforschung Dresden e.V., Dresden, Germany

[2]Technische Universität Dresden, Faculty of Chemistry and Food Chemistry, Dresden, Germany

[3]Université de Lyon, École Normale Supérieure de Lyon, Université Claude Bernard, CNRS, Laboratoire de Physique, F-69342, Lyon, France

[4]Fraunhofer-Institut für Angewandte Polymerforschung, Potsdam-Golm, Germany

[5]Technische Universität Dresden, Institute for Theoretical Physics, Dresden, Germany

*Correspondence: yong@ipfdd.de (H.Y.); fabien.montel@ens-lyon.fr (F.M.); sommer@ipfdd.de (J.-U.S.)

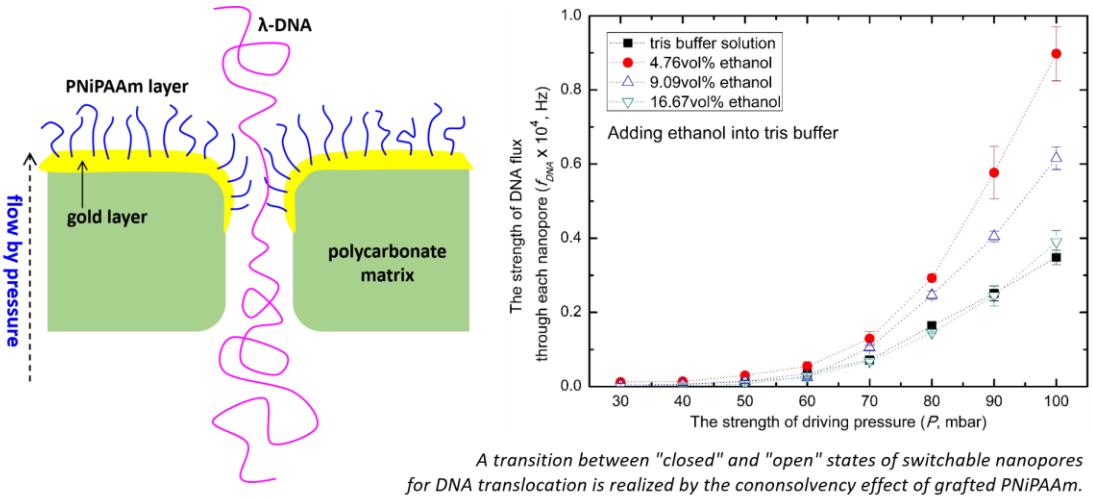

A transition between "closed" and "open" states of switchable nanopores for DNA translocation is realized by the cononsolvency effect of grafted PNiPAAm.

Abstract

Stimulus response of polymer-decorated nanopores/nanochannels is a fascinating topic both in polymer science and modern nanotechnology; however, it is still challenging for standard analytical methods to characterize these switchable nanopores/nanochannels. In this study, based on the physics of polymer translocation we developed an analytic method and thus for the first time were able to quantitatively measure the effective thickness of the polymer layer around the rim of nanopores. As an application example of this method, we studied the translocation dynamics of fluorescence DNA through poly(N-isopropylacrylamide) decorated switchable nanopores in aqueous environments. By adding small amounts of ethanol to the

aqueous buffer solution a switch-like response of the DNA-translocation can be observed. It is also observed that a pronounced switching effect can be only realized in a window of moderate grafting densities of poly(N-isopropylacrylamide) layer. These are attributed to the cononsolvency effect which causes a collapse of the polymer layer and thus a transition between "closed" and "open" states of the nanopores for DNA translocation. Our study clearly transpired that cononsolvency effect of polymers can be used as a novel trigger to change the size of nanopores, in analogy to the opening and closure of the gates of cell-membrane channels. We envisage that our study will spawn further developments for the design of switchable nano-gates and nanopores.

1. Introduction

Switch-like response in soft matter can be achieved by volume changes of immobilized polymers such as gels and polymer brushes in solution, triggered by pH, thermal and photo responses **[1]**. However, harnessing of these effects in applications generally requires a large change of the environmental parameters such as temperature and pH. Particularly when considering applications in biomaterials this is inconvenient, since in living environments temperature and pH usually has to be controlled in a narrow range. On the other hand, it is known that volume phase transitions take place when biopolymers such as RNA are mixed with multicomponent solutes/solvents including non-specifically RNA-binding proteins **[2, 3]**. Another example is a re-entrance condensation of proteins in aqueous solutions observed by addition of multivalent salts **[4]**. A phenomenon similar to re-entrance condensation of proteins is cononsolvency first observed in synthetic polymers **[5, 6]**. Here, a mixture of two good solvents causes the collapse or demixing of polymers such as poly(N-isopropylacrylamide) (PNiPAAm) in a certain range of compositions of these two solvents. It is worth noting that this transition is of first order even for immobilized macromolecules **[7]**, thus a small concentration change of the cosolvent is sufficient to trigger the collapse. Previous studies **[8]** confirmed that the thickness of a PNiPAAm brush on a flat surface exhibits a switch-like response when a very small amount of alcohol (usually termed as cosolvent) is added into the aqueous solutions of polymer brushes. Thus, cononsolvency of polymer brushes appears as a promising candidate to mimic the opening and closing of cell-membrane channels, but so far this is merely supported by coarse-grained computer simulations **[9-11]** and not yet reported in any experimental investigation **[12-15]**.

Meanwhile, we have to realize that it is impossible to do a rational experimental investigation on the cononsolvency response of polymer-decorated switchable nanopores, unless suitable characterizing methods are available. However, it remains very challenging for standard analytical methods to characterize stimulus-responsive behaviors of polymer layers in various confined environments such as nanopores. To our best knowledge, only few studies **[16-18]** reported that the atomic force microscopy can be used to qualitatively detect

the hydrodynamic thickness of a polymer layer around the hollow structures. Lack of analytic methods to quantify the thickness of a polymer layer around the rim of nanopores, actually impedes further developments for the rational design of functionalized nano-gates and nanopores **[12-15, 19-21]** for applications such as the sensing of single molecules **[22-27]**.

Hence it is an important aim of this work to develop a method to quantitatively determine the thickness of polymer layer around the rim of nanopores. In this study we achieved this task on the basis of the physics of polymer translocation**.** As an application example of this method, we studied the translocation dynamics of fluorescence DNA through PNiPAAm decorated switchable nanopores in aqueous environments. We demonstrated that switchable nanopores can be prepared by harnessing the cononsolvency transition in grafted polymers. The widening of the PNiPAAm decorated nano-channels occurs in a narrow window of about 5% volume fraction of ethanol in aqueous buffer solution. Experimental results quantitatively showed that PNiPAAm layers around the rim of nanopores show solvent-composition responsive behaviors in the range of metabolic pH values and room temperatures. In the following, the methodology used in this study will be firstly described in **Section 2**, then experimental results will be discussed in **Section 3** and finally concluding remarks will be made in **Section 4**.

2. Experiments and Methods

2.1. DNA translocation experiments

In our experiments, track-etched polycarbonate membranes (Whatman, with nominal pore diameters equal to $50nm$ and thicknesses equal to $6\mu m$) were used in DNA translocation experiments. First the membranes are one-side sputtered with a thin layer of gold (EVA 300 Alliance Concept evaporator, thickness 50 nm, speed of deposit 0.2 nm). A typical scanning electron microscopy image of the gold-coated nanopores used in DNA translocation experiments in this study is shown in **Figure 1**. The polydispersity of the sizes of the nanopores is rather low, the boundary for the diameter is about 50±10nm, similar nanopores were already used in our previous investigations **[28]**. Then the gold layer is grafted with a PNiPAAm layer by grafting-to synthetic method. In this study, the different samples are named as "higher-graft-15K" and "lower-graft-15K" to discriminate the higher and lower grafting densities of polymer layers with a molecular weight of M_n = 1.5 x 10^4 g/mol, and dispersity M_w/M_n = 1.18. We named "higher-graft-30K" and "lower-graft-30K" to discriminate the higher and lower grafting densities of polymer layers with a molecular weight of M_n = 3.0 x 10^4 g/mol, and dispersity M_w/M_n = 1.25. For the details of preparing these polymer layers,

see **section S1.1** of **Supporting Materials**.

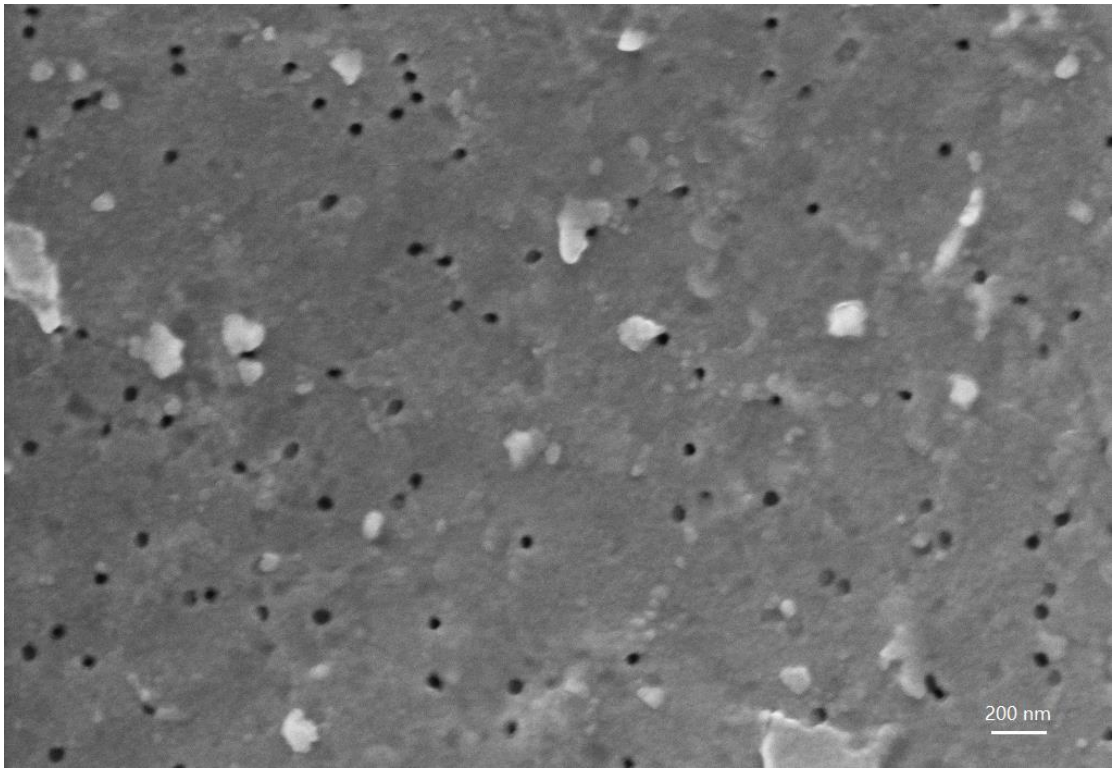

Figure 1. A typical scanning electron microscopy image of the gold-coated nanopores used in DNA translocation experiments in this study. The dark circles in the image are nanopores.

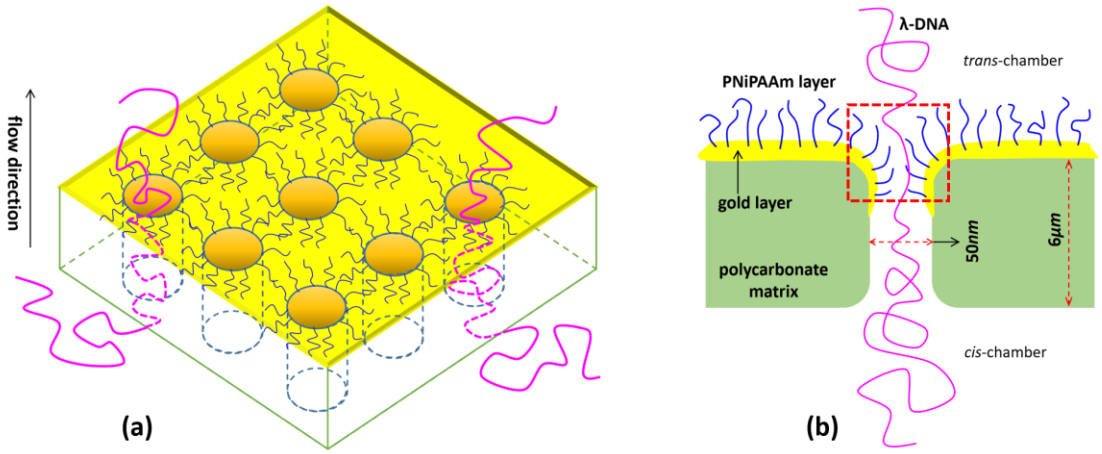

Figure 2. A sketch of fluorescence λ-DNAs translocating through PNiPAAm-grafted nanopores: (**a**) three-dimensional view of nanopore structures, and (**b**) side view of a single nanopore. In this study, based on the DNA-translocation efficiency we developed an analytic method to quantitatively measure the effective thickness of a polymer layer around the rim of nanopores, i.e., the polymer layer in the box region depicted in the **Figure 2b**.

As for DNA translocation experiments, a dilute solution of λ-DNA (0.1 pM, 48 kbp) in tris buffer solution (tris 10 mM, EDTA 1 mM and KCl 10 mM, pH ≈ 7.6) fluorescently labeled with

YoYo-1 (Life Tech) filled in the *cis*-chamber where the pressure was applied, for the experimental details please refer to our previous publications such as **ref.[28]**. A few hundred DNA translocation events were observed simultaneously with a time resolution of about 10ms by fluorescence microscopy, which was sufficient to resolve each translocation event. A cartoon depiction of λ-DNAs translocating through PNiPAAm-grafted nanopores, is shown in **Figure 2**.

In our cononsolvency experiments, ethanol is merely added to the buffer solution in the *trans*-chamber, see **Figure 2b**. It is worth noting that the volume size of the *trans*-chamber is significantly larger than that of the *cis*-chamber; thus, in our study, the solvent-composition change in the *trans*-chamber due to buffer solutions (without ethanol) driven from the *cis*-chamber can be neglected.

Because the *trans*-side of the membrane including a part of the nanochannel is coated with a gold layer, the direct contact between solvent and polycarbonate matrix in the *trans*-side is actually blocked and the infiltration of ethanol on polycarbonate matrix unlikely happens when taking into account that the pressure on the *cis*-side of the membrane causes a flow from the *cis*- to the *trans*- chambers. Thus, it is unlikely that the DNA translocation in the nanochannel is directly affected by the addition of ethanol in the *trans*-chamber. This was confirmed by our control experiments for blank membrane (without grafting PNiPAAm layers) in various mixtures of ethanol and tris buffer, for details see **section S2** of **Supporting Materials**. In addition, the analytic method to determine the thickness of nanopore brushes that we developed in this work (see **section 2.2**) relies on the system at a steady state under the flow pressure from the *cis*- to the *trans*- chambers. Before collecting data, it is necessary to wait a period of time to make sure the system is at steady state when the driving pressure is changed in experiments. In our experiments this waiting time is about two minutes. This approach also can help to effectively eliminate the possible influence of ethanol infiltration on the polycarbonate nanochannel in our cononsolvency experiments.

Although ethanol addition obviously affects the DNA conformation in the *trans*-chamber (after translocation) when the volume faction of ethanol is high (the threshold value is about 40% in our study when the solvent becomes poor for DNA), we note that the most interesting effects occur for very low ethanol concentrations far below the threshold value of 40%. The poorer solvent quality in the *trans*-chamber implies a chemical potential or solubility gradient acting against the translocation. Since we see a clear re-entrance behavior at higher alcohol concentrations this effect is apparently only of minor importance for the observation of the gating behavior of the pores.

2.2. Characterizing the effective thickness of a grafted polymer layer around the rim of nanopores

In this study, to quantitatively estimate the thickness of the polymer layer around the rim of nanopores, we used the celebrated suction model for the translocation of polymer in dilute solutions introduced by P.-G. de Gennes **[29, 30]**. Our method is on the basis of the DNA-translocation efficiency which in turn relies on the proven fact that in the strong confinement regime, the critical force to guide flexible linear polymer chains through nanopores is independent of the chain length **[31]**. We analyzed the variation of the DNA translocation frequency per pore (f_{DNA}) with the driving force such as the gradient of flow pressure, see **Figure 2b**. In the framework of the suction model **[28, 32]**, the translocation frequency is expressed as

$$f_{DNA} = k_1 \exp(-\frac{\Delta F}{k_B T}), \quad (1)$$

by assuming that DNA translocation is described as the travel of a flexible polymer through a free-energy landscape with a barrier of height ΔF and assuming the translocation process follows a Boltzmann statistic. We note that the persistence length of DNA is about 50 nm which is also the nanopore size in this study, thus a flexible-polymer-chain assumption for DNA in this study is reasonable **[33]**.

In **Eq.(1)**, k_B is the Boltzmann constant and T is the thermodynamical temperature. k_1(Hz) is the rate of incidence on the barrier. By Kramers' theory **[34, 35]** for Brownian motion in a field of force, when k_1 is dominated by the presence of the barrier ΔF, $k_1 \propto J/J_c$ holds with J the solvent flux ($m^3\ s^{-1}$) and J_c the solvent-flux threshold. In the suction model, the energy barrier is $\Delta F = k_B T(J_c/J)$ and the translocation frequency f_{DNA} finally reads

$$f_{DNA} = k_2 \left(\frac{P}{P_c}\right) \exp(-\frac{P_c}{P}), \quad (2a)$$

with k_2 a proportionality factor (Hz), P the gradient of pressure applied by the equipment where the pressure on the side of membrane without coating a gold layer is higher, the critical pressure $P_c = r_h J_c$. The hydrodynamical resistance of the pore r_h equals to $8\eta L/\pi R^4_{eff}$ with L the length of a pore ($L = 6\mu m$ in this study) by Poiseuille's law, R_{eff} is the effective radius of pores, and η is the solvent viscosity in the *cis*-chamber, see **Figure 2b**. In this study, η is the solvent viscosity of the tris buffer (without ethanol).

Taking into account of that the pore size is significantly larger than the cross-sectional size of DNA backbone and the Reynolds number is at the order of about 10^{-4}, the Poiseuille's law and Darcy's law are still valid for the flow in this study **[28, 36]**. Keeping in mind that the solvent-flux threshold (J_c) of polymer translocation has been proven by both theories **[29, 30]** and experiments **[31]** at the order of

$$J_c = const \times \frac{k_B T}{\eta}, \tag{3a}$$

then we can use this relation to estimate the thickness of a polymer layer around the rim of nanopores. Technically speaking, it is unnecessary to know the numerical prefactor on the right-hand side of **Eq.(3a)** in experiments; the effective (hydrodynamic) radius of the polymer-decorated pore, R_{eff}, can be calculated in a way of avoiding the numerical prefactor as below,

$$R_{eff} = R_0 \left(\frac{P_{c,0}}{P_{c,eff}} \times \frac{T_{eff}}{T_0} \right)^{\frac{1}{4}}, \tag{4a}$$

where $P_{c,0}$ and $P_{c,\ eff}$ are critical pressures of the blank membrane and when the same membrane is grafted with a polymer layer, respectively; T_0 and T_{eff} are temperatures where experiments are conducted for the blank membrane and when the same membrane is grafted with a polymer layer, respectively. In our cononsolvency experiments, the temperature is fixed at 298K; thus, $T_{eff} = T_0$ holds in our experiments. R_0 is the radius of nanopores without grafted polymers, usually it is insensitive to normal temperature change, in this study R_0 = 25.0±1.0 nm is the corresponding measured mean value with an average absolute deviation using scanning electron microscopy (**Figure 1**).

Taking into account the fact that the polymer layer grafted around the rim of nanopores, the relation of $R_{eff} \leq R_0$ always holds. Then, the effective thickness of the polymer layer around the rim of nanopores can be obtained as

$$H = R_0 - R_{eff}, \tag{5}$$

i.e., the effective thickness of the polymer layer in the box region depicted in **Figure 2b**. It is remarkable that **Eq.(4a)** is a fourth-order power law, this implies that the change of critical pressure is sensitive to the change of pore size and thus the effective thickness of the polymer layer around the rim of nanopores can be estimated in a relatively high accuracy. It is noted

that we measure H under flow conditions which leads to that the estimated thickness (H) may not coincide with the thickness of equilibrium polymer layers.

The DNA translocation frequency per pore f_{DNA} is calculated as

$$f_{DNA} = \frac{N_{DNA}}{\rho_{pore} A t} . \tag{6}$$

The DNA-translocation efficiency, i.e., the number of DNA translocation events (N_{DNA}) through a fixed area (A =135μm x 135μm) of membranes and in a fixed period of time (t = 30 s) that observed in the *trans*-chamber is counted both by a combination of visual inspection by human eyes and using an in-house script coded in Python. Examples to determine the number of DNA translocation events are shown in **Figure S1** of **Supporting Materials** and **Video Supporting Materials**. For the details how to count the number of DNA translocation events and process these data, see **sections S1.2-1.4** of **Supporting Materials**.

The pore density in **Eq.(6)** is with a value of ρ_{pore} = 6 x 10^8 pores/cm^2 in this study. The average number of pores in the fixed area is about 1.1 x 10^5, thus the observed number fluctuation of DNA translocation events in this study actually can be neglected. As shown in **Eq.(6)**, the number of translocation events (N_{DNA}) observed in this study only differs from the translocation frequency (f_{DNA}) by a constant multiplicatory factor. In this study the critical pressure (P_c) is obtained by fitting the nonlinear equation **Eq.(2a)**, the detail of using **Eq.(2a)** to process experimental data in this study is shown in **section S1.4** of **Supporting Materials**.

We note that the driving force for DNA translocation through nanopores/nanochannels can be an electric field **[19, 37]** which is widely used in translocation experiments and still lack of quantitative methods to characterize, our experimental method can be extended and formulated to this case. Following a rationale in analogy to the case of pressure driving as shown above, for the case of electric field as the driving force, the translocation frequency f_{DNA} reads as **[38]**,

$$f_{DNA} = k_3 \left(\frac{E}{E_c} \right) \exp(-\frac{E_c}{E}) , \tag{2b}$$

with k_3 a proportionality factor (Hz), E the strength of the electric field applied to drive DNA

translocation and E_c the electric-field threshold. In experiments, the voltage strength $V = EL$ is usually used instead of the electric-field strength (E) with L the length of a pore (such as $L = 6\mu m$ in this study).

It is remarkable that from experimental observations **[28, 38-40]**, DNA-translocation behaviour can be qualitatively separated by the free energy barrier of translocation into two distinct regimes. When the driving force is lower or comparable to the free energy barrier, diffusive and slow dynamics can be approximated by an exponential increase with the external force. When the driving force is significantly larger than the free energy barrier, it asymptotically approaches to a linear increase. This heterogeneous behaviour is also verified by the hydrodynamic derivation of **Eq.(2a)** and **Eq.(2b)**. The applicability of **Eq.(2b)** can be verified by experimental data reported by **refs.[38-40]**. It is worth noting that one can estimate the free energy barrier for a successful polymer translocation by using **Eq.(2a)** and **Eq.(2b)**; it is at the order of several k_BT and agrees with the prediction of the scaling theory as already reported in our previous work **[28]**.

For the case of electric field as the driving force, the electric-field threshold (E_c) to overcome the free energy barrier of polymer translocation is bias equivalent to the critical flux in the suction model and is scaled at the order of

$$E_c = const \times \frac{k_B T}{qR^3}, \tag{3b}$$

with R the pore radius **[38]**. Taking into account of that for controlled experiments the surface charge density (q) of polymer "blobs" in the nanopore usually is a constant and insensitive to normal temperature change; the effective (hydrodynamic) radius of the polymer-decorated pore, R_{eff}, can be calculated in a similar way like **Eq.(4a)**,

$$R_{eff} = R_0 \left(\frac{E_{c,0}}{E_{c,eff}} \times \frac{T_{eff}}{T_0} \right)^{\frac{1}{3}}, \tag{4b}$$

where $E_{c,0}$ and $E_{c,\,eff}$ are electric-field thresholds of the blank membrane and when the same membrane is grafted with a polymer layer, respectively. Note that the exponent difference between **Eq.(4a)** and **Eq.(4b)**, it implies that a pressure-controlling experiment is preferable; because comparing with the change of electric-field threshold, the change of critical pressure is much sensitive to the change of pore size. Nevertheless, one advantage of translocation

experiments by electric-field driving is that the translocation frequency (f_{DNA}) can be easily and accurately obtained via the analysis of electric-current signals with respect to time trace.

Let us mention that our experimental method is an ensemble-average approach and the statistical quality of the results depends on a sufficiently high pore-density in the membrane. The basic assumption of our method is that the DNAs have a radius of gyration larger than the pore diameter and they are in the dilute regime of the DNA solution. We also note that in the translocation experiments, other polymers can be also used such as proteins **[23-25]** and synthetic polymers **[41, 42]**, in principle our experimental methods can be extended without difficulty to these cases; however, this topic is beyond the scope of this study.

3. Results and Discussion

3.1. Results of DNA flux through (PNiPAAm-decorated) nanopores

Our experimental results of the translocation frequency of DNA per pore in a tris-buffer solution as a function of pressure are displayed in **Figure 3**. We compare the results for blank membranes (with a gold layer) and for different grafting densities of PNiPAAm. For different grafting densities the translocation efficiency, i.e., the translocation frequency of DNA per pore at a given pressure, is reduced dramatically as compared to the bare or blank membrane. At higher pressure the higher grafting density leads to a higher reduction of the translocation efficiency in accordance with the fact that higher grafting densities lead to thicker polymer layers when the chain lengths of grafted polymers are the same. With the help of a scaling analysis, we can show that the polymer layers displayed in **Figure 3a** are in a brush state, while the polymer layers displayed in **Figure 3b** are below the brush state; for the details see **section S1.5** of **Supporting Materials**.

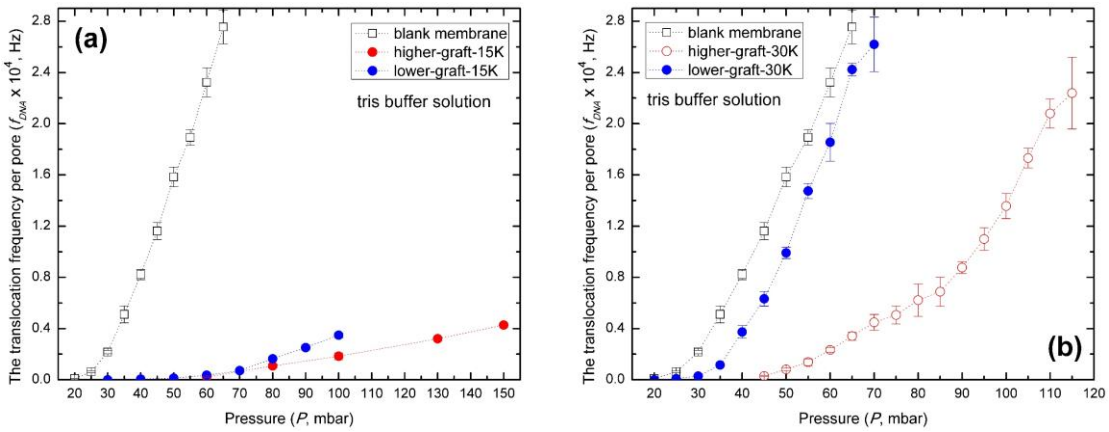

Figure 3. The translocation frequency of DNA per pore with respect to pressure. (**a**) Grafting-density effect of different PNiPAAm layers with a shorter polymer chain in tris buffer, the molecular weight of PNiPAAm layers is M_n = 1.5 x 10^4 *g/mol*, and dispersity is M_w/M_n = 1.18. (**b**) Grafting-density effect of different PNiPAAm

layers with a longer polymer chain in tris buffer, the molecular weight of PNiPAAm layers is M_n = 3.0 x 10^4 *g/mol*, and dispersity is M_w/M_n = 1.25. pH value of the buffer is about 7.6 and measurement temperature is at 25 °C. The dotted lines in the figures are guides to eyes.

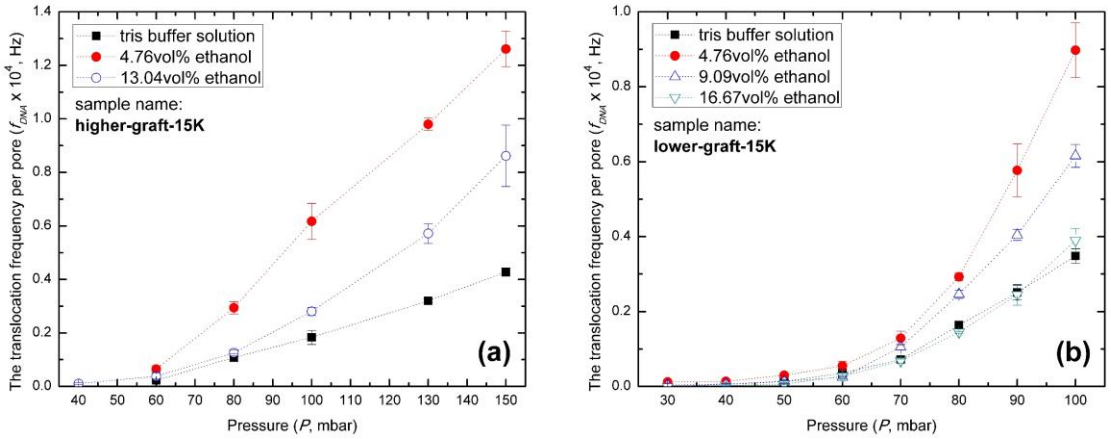

Figure 4. The translocation frequency of DNA per pore with respect to pressure. Solvent-composition response of different PNiPAAm layers: (**a**) for a membrane of a higher grafting density, and (**b**) for a membrane of a lower grafting density. The molecular weight of PNiPAAm layers is M_n = 1.5 x 10^4 *g/mol*, and dispersity is M_w/M_n = 1.18. pH value of the buffer is about 7.6 and measurement temperature is at 25 °C. The dotted lines in the figures are guides to eyes.

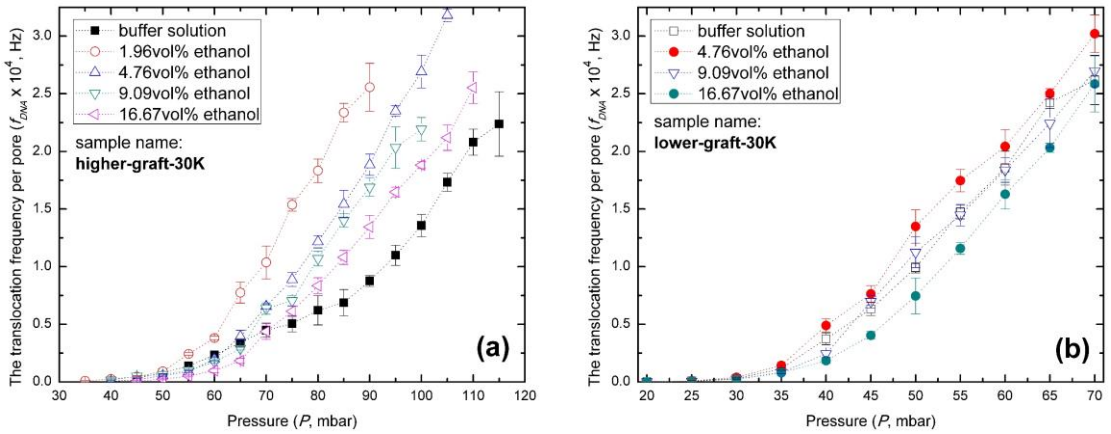

Figure 5. The translocation frequency of DNA per pore with respect to pressure. Solvent-composition response of different PNiPAAm layers: (**a**) for a membrane of a higher grafting density, and (**b**) for a membrane of a lower grafting density. The molecular weight of PNiPAAm layers is M_n = 3.0 x 10^4 *g/mol*, and dispersity is M_w/M_n = 1.25. pH value of the buffer is about 7.6 and measurement temperature is at 25 °C. The dotted lines in the figures are guides to eyes.

As shown in **Figures 4** and **Figures 5**, for each membrane with a PNiPAAm layer, the translocation frequency of DNA per pore first increases with an increase of ethanol

concentration. With further increasing ethanol concentration, the translocation frequency of DNA per pore decreases again. This implies the size of the nanopores firstly increases under the stimuli of increasing ethanol concentration, later the nanopore size reduces by further increasing ethanol concentration. This indicates that grafted PNiPAAm shows re-entrance signature of cononsolvency transition in the ethanol/tris-buffer mixtures, as observed for flat brushes **[8]**. This observation is clearly supported by a study of the normalized translocation frequency of DNA per pore which is plotted with respect to the change of ethanol concentration under different driving pressures, see **Figure 6** and **Figure S5** (**Supporting Materials**). Solvent-composition responsive behaviors shown in **Figures 4-6** and **Figure S5** indicate that the cononsolvency effect of grafted PNiPAAm can be used to control the size of nanopores.

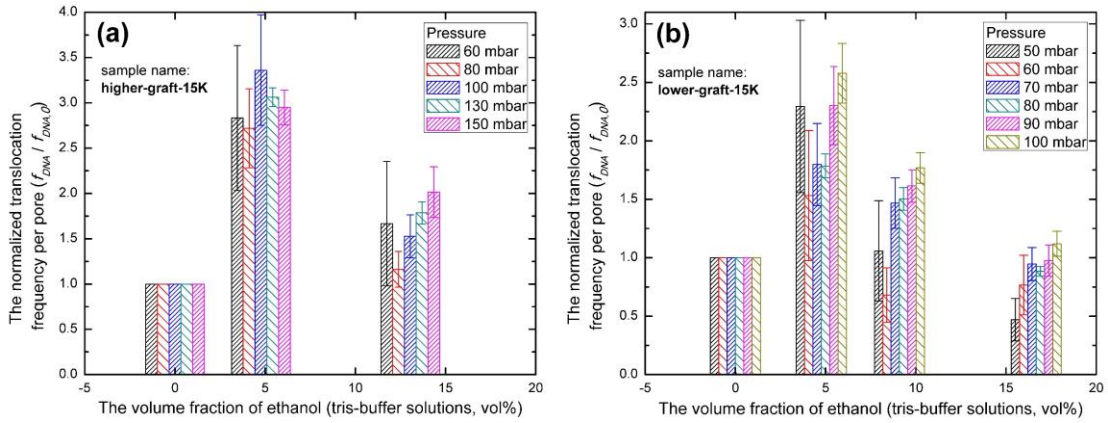

Figure 6. The normalized translocation frequency of DNA per pore is plotted with respect to ethanol concentration change under different driving pressure. (**a**) For a higher grafting density of PNiPAAm-grafted nanopores, data are the same as in **Figure 4a**. (**b**) For a lower grafting density of PNiPAAm-grafted nanopores, data are the same as in **Figure 4b**. Note that $f_{DNA,\,0}$ is the observed translocation frequency of DNA per pore in tris buffer solutions (no addition of ethanol). From the left-hand to the right-hand sides of the figure, column bars arrange the pressure in increasing order.

In **Figure 4b** and **Figure 5a**, it is noted that for polymer layers with moderate-grafting densities, when the applied flow pressure is low and in a certain range, DNA can translocate through PNiPAAm-decorated nanopores at very low concentrations of ethanol (4.76%vol and 1.96%vol, respectively) but not at much higher concentrations of ethanol and in tris buffer. This phenomenon is unavoidably attributed to the cononsolvency effect which causes a collapse of the polymer layer and thus a transition between "closed" and "open" states of the nanopores for DNA translocation. Under the condition of flow pressure, a depiction of DNA translocation and ethanol-concentration induced phase transition of a PNiPAAm layer around the rim of nanopores, is shown in **Figure 7**.

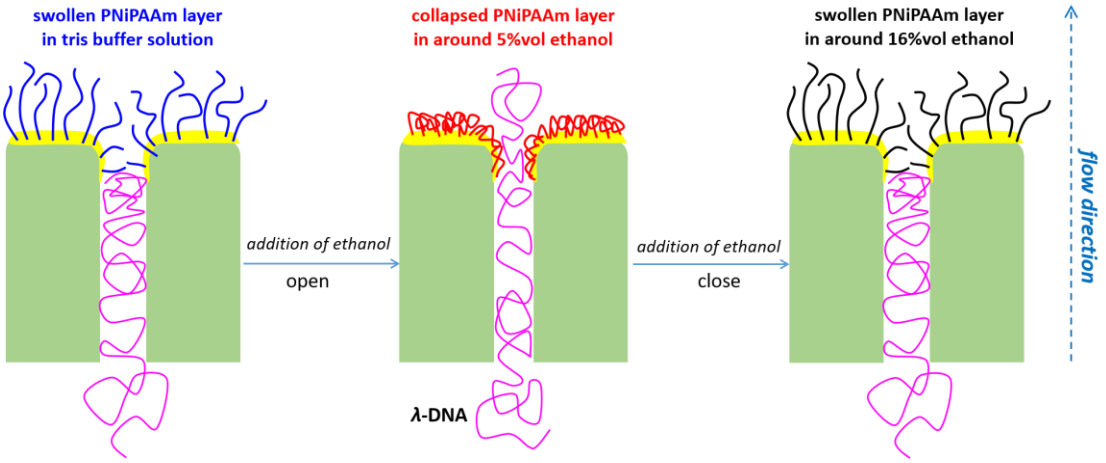

Figure 7. For a polymer layer with a moderate-grafting density, when the applied flow pressure is low and in a certain range, the DNA translocation through PNiPAAm-decorated nanopores can be regulated by the addition of ethanol to tris buffer solutions. This phenomenon is attributed to the cononsolvency effect which causes a collapse of the polymer layer and thus a transition between "closed" and "open" states of the nanopores.

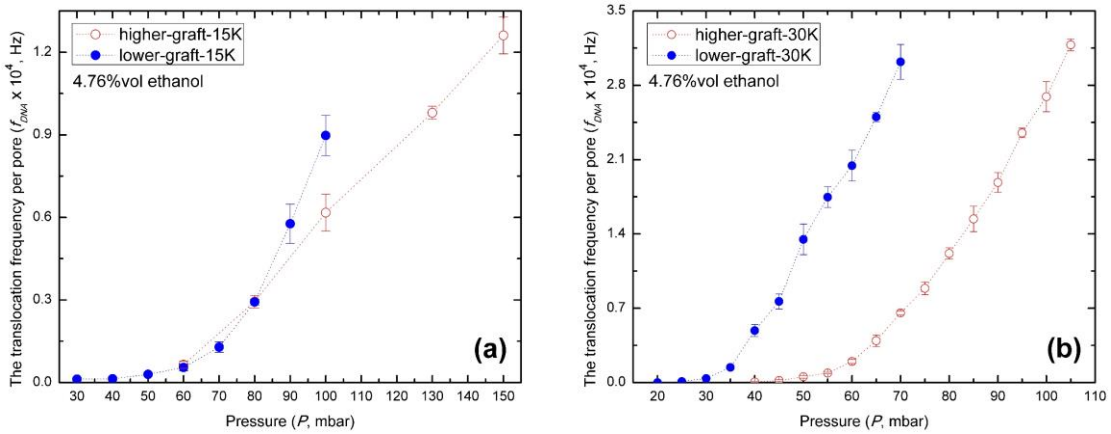

Figure 8. The translocation frequency of DNA per pore with respect to pressure. Grafting-density effect of different PNiPAAm layers in 4.76%vol ethanol-tris buffer mixtures when DNAs translocate through nanopores. (**a**) Membranes with the molecular weight of PNiPAAm layers M_n = 1.5 x 10^4 *g/mol*, and dispersity is M_w/M_n = 1.18. (**b**) Membranes with the molecular weight of PNiPAAm layers M_n = 3.0 x 10^4 *g/mol*, and dispersity is M_w/M_n = 1.25. pH value of the buffer is about 7.6 and measurement temperature is at 25 °C. The dotted lines in the figures are guides to eyes.

In **Figure 8**, we display the results for both grafting densities at the opening of PNiPAAm-grafted nanopores at 4.76%vol of ethanol. Comparing results for both grafting densities in tris buffer (**Figure 3**) and 4.76%vol of ethanol (**Figure 8**), we observe a consistent increase of DNA translocation efficiency with decreasing grafting density of the polymer layer. We made

control experiments for nanopores which had no grafted PNiPAAm and verified that the direct effect of ethanol on the translocation behavior of DNA was actually negligible, see **Figure S6** (**Supporting Materials**); as well as ethanol has no swelling effect on the matrix material (gold-coated polycarbonate) used to manufacture nanopores in this study. It should be particularly pointed out that the observed re-entrance behaviors of DNA translocation in **Figures 4** and **Figure 5** can hardly be ascribed to the possible infiltration of ethanol on the polycarbonate nanochannels, because the ethanol infiltration can merely lead to a monotonous change with an increase of ethanol concentration and therefore the re-entrance behaviors of DNA translocation shall not be observed at all on account of ethanol infiltration. Therefore, the origin of the non-monotonous opening/closing behavior of the nanochannel can be merely the solvent response of the grafted PNiPAAm. These results are in agreement with our previous studies of flat brushes, where a non-monotonous change of the brush height is with a minimum at low alcohol concentrations **[8]**.

Let us add some remarks about the effect of polydispersity of bare pore size on our results. The polydispersity of the bare membrane in our study is rather low (with a boundary of diameter about 50±10nm, see **Figure 1**) and thus smaller or larger pores should not lead to a qualitatively different translocation behavior. Nevertheless, a priori averaging over all translocation events through the membrane reduces the contrast between "open" and "closed" pores in the cononsolvency response. Thus, our ensemble-averaged measurements give a lower boundary for the quality of the switching response which could be achieved under ideal monodisperse condition. An interesting and maybe somewhat counter-intuitive conclusion can be drawn from the interplay between the grafting-to synthetic method and the variation of bare pore size: Since larger pores lead to less geometric constraints for the polymer grafting reaction, a higher grafting density and thus a larger height of the resulting polymer layer can be expected. This reduces the effective size variation of the polymer-coated pores.

3.2. A comparative study between nanopore brushes and flat brushes

Whilst our experimental results of DNA flux through nanopores are in agreement with our present understanding of the cononsolvency effect in grafted polymer layers for flat surfaces, the above discussions are still qualitative so far. To get some quantitative insights, we used the experimental results in **Figures 3-5** to calculate the reference values for the absolute height of PNiPAAm layers around the rim of nanopores using **Eq.(2a)**, **Eq.(4a)** and **Eq.(5)**, the results are displayed in **Table 1.** The grafting densities and morphological regimes of polymer layers in this study were also estimated, see **Table 1**; for the details see **section S1.5** of **Supporting Materials**.

Table 1. The reference values for the swollen thickness of PNiPAAm layers around the rims of nanopores in

mixtures of tris buffer added with various concentrations of ethanol. The layer thickness and its error bars are calculated based on the data of the translocation frequency of DNA per pore reported in **Figures 3-5**. These data are calculated by the analytic method developed in this study, for details see **section 2.2**.

sample name	**grafting density** ($chains/nm^2$)	**Tris buffer** (nm)	**1.96%vol** (nm)	**4.76%vol** (nm)	**9.09%vol** (nm)	**13.04%vol** (nm)	**16.67%vol** (nm)	**morphology**
higher-graft-15K	~ 0.30	10.0 ± 1.0	/	8.5 ± 0.1	/	9.0 ± 0.5	/	brush
lower-graft-15K	~ 0.15	7.0 ± 0.1	/	3.8 ± 0.1	6.3 ± 0.1	/	7.5 ± 0.5	brush
higher-graft-30K	~ 0.05	5.3 ± 0.1	3.5 ± 0.1	4.3 ± 0.1	4.2 ± 0.1	/	4.5 ± 0.1	mushroom/brush*
lower-graft-30K	<< 0.05	1.6 ± 0.1	/	1.2 ± 0.1	1.4 ± 0.1	/	2.1 ± 0.1	mushroom

*It is hard to determine the exact morphology for this sample merely based on a scaling analysis.

In **Figure 9**, we also display the normalized swollen thickness of polymer layers which are grafted around the rim of nanopores. It is observed that in **Figure 9a** an increase of grafting density of nanopore brushes, weakens the collapse transition of brush layer in ethanol/tris buffer mixtures, this follows the analytic prediction of a mean-field model for cononsolvency transition by our previous studies **[7, 43]**. As well as shown in **Figure 5b** and **Figure 9b,** a PNiPAAm polymer layer with very low grafting density below the brush state still displays re-entrance behavior; however, corresponding phase-transition behaviors are not pronounced. It becomes clear that a pronounced switching effect can only be realized in a window of moderate grafting densities.

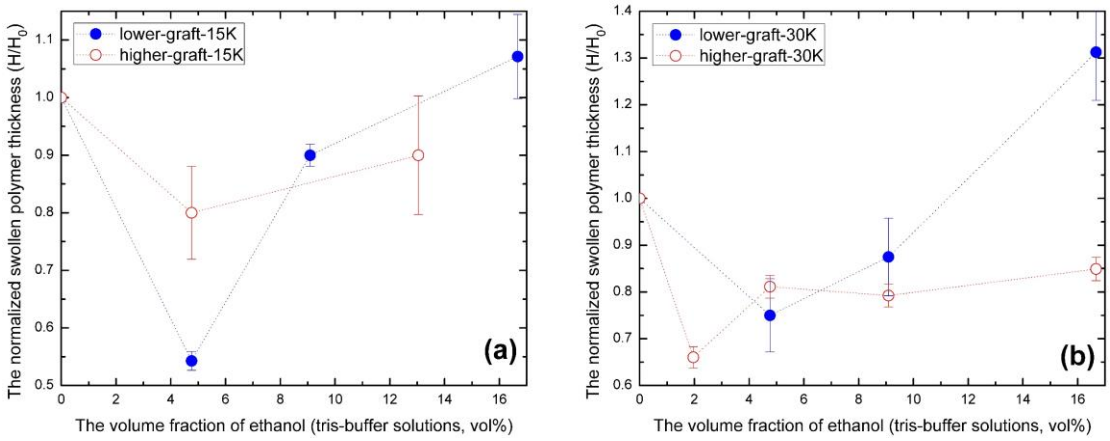

Figure 9. The ethanol-concentration response of grafted PNiPAAm polymers around the rim of nanopores, the relative polymer thickness is calculated by the data reported in **Table 1**. (**a**) Membranes with the molecular weight of PNiPAAm layers M_n = 1.5 x 10^4 g/mol, and dispersity M_w/M_n = 1.18. (**b**) Membranes with the molecular weight of PNiPAAm layers M_n = 3.0 x 10^4 g/mol, and dispersity M_w/M_n = 1.25. pH value of the buffer is about 7.6 and measurement temperature is at 25 °C. The dotted lines in the figures are guides to eyes.

From **Figure 9b**, we observed that a decrease of grafting density weakens the collapse regarding the normalized swollen polymer thickness, in contrast to the behavior shown in

Figure 9a. The reason behind this observation is that the grafting-to synthetic approach leads to much lower grafting densities for the high-molecular-weight polymers, see the second column of **Table 1**. This in turn leads to particular morphologies in the collapsed state such as octopus-shape micelles or collapsed globules **[44-47]**, see the last column of **Table 1**. In turn the hydrodynamic thickness variation of such sparsely grafted polymer layers displays only weak variation as compared with the dense brush regime. Nevertheless, it is interesting to observe that regardless of whether the polymer layer is in a brush state, the grafting density has only a very small effect on the solvent-composition location of the maximum collapsed state. All these above-mentioned cononsolvency behaviors are also observed for grafted PNiPAAm polymers on flat surface both in ethanol/water mixtures **[8]** and in ethanol/tris buffer mixtures, see **Figure S7** and **Figure S8** (**Supporting Materials**).

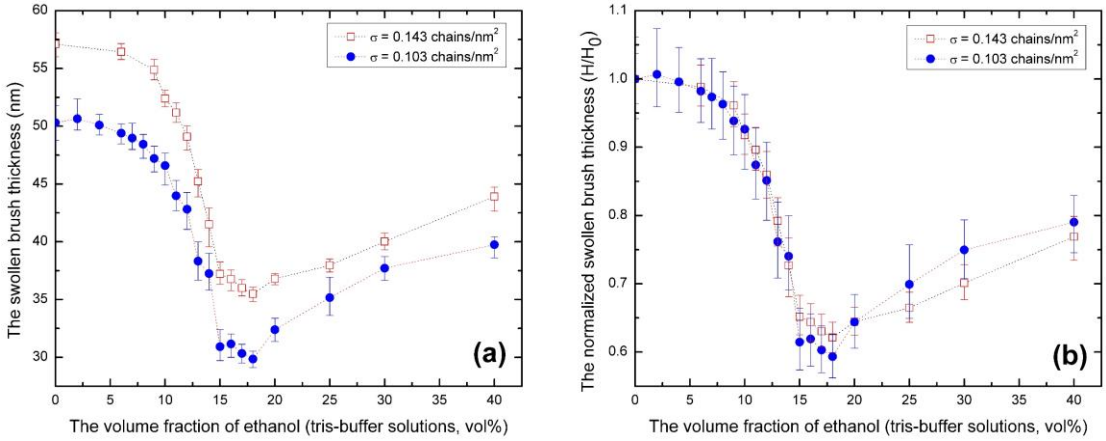

Figure 10. A study of in-situ Vis-spectroscopic ellipsometry for equilibrium swollen brush thickness on grafting-density effect in the cononsolvency transition of PNiPAAm brushes in ethanol/tris buffer mixtures on the flat surface, at the temperature of 25°C, the pH value of the buffer is 7.45: (a) absolute swollen brush thickness, (b) normalized swollen brush thickness. Experiments were conducted with the molecular weight of $M_n = 6.1\times10^4$ g/mol, $M_w/M_n = 1.40$ for all polymer brushes. The dotted lines in the figures are guides to eyes.

Figure 10 shows measurements of in-situ Vis-spectroscopic ellipsometry for equilibrium swollen thickness of two PNiPAAm brushes with different grafting densities on flat surface which are immersed in tris-buffer/ethanol mixtures, for more results also see **Figures S8-S10** (**Supporting Materials**). The methods of preparing these flat brushes and conducting ellipsometry experiments were reported in our previous studies **[48]**. The ellipsometry study clearly indicates that PNiPAAm brushes undergo a collapse with respect to an increase of ethanol concentration; as well as at higher concentration of ethanol, the PNiPAAm brushes show re-entrance behavior. It also indicates that an increase of grafting density of PNiPAAm flat brushes, weakens the collapse transition of flat brushes in ethanol/tris buffer mixtures provided that the collapsed brush displays a homogeneous morphology. In addition, it is of interest to see that from the right branch of the re-entrance transition for the relative brush

thickness (**Figure 9a** and **Figure 10b**), both nanopore brushes and flat brushes show similar re-entrance behaviors regarding the change of grafting density. These ellipsometry observations qualitatively cross-verified our DNA translocation experiments.

From the comparison of **Figure 9** and **Figure 10**, it should however be noted that the phase-transition window detected by translocation experiments through nanopores under non-equilibrium conditions differs from the window detected by ellipsometry experiments at equilibrium states. The reason for this discrepancy may be attributed to the fact that the brush is subjected to flow fields, osmotic pressure induced by the translocating DNA and hydrostatic pressure effects. From the theoretical description of the cononsolvency transition in brushes and in solutions **[7, 49]**, it is known that densification of the polymer due to external forces shifts the cononsolvency transition to smaller cosolvent (ethanol) concentrations. It is worthy of addressing that from the comparison of **Figure 9a** and **Figure 10b**, it can be seen that despite of the shift in the transition window, the reduction of relative height in the flat brush corresponds the change of the radius of the polymer-grafted nanopore when the grafting density is at the same level, see the data of blue circles in **Figure 9a** and data in **Figure 10b**, this can be analytically predicted by our previous theoretical studies for brush layers **[7, 43]**; readers who are interested in theoretical details, please refer to our previous publications **[7, 43]**.

4. Conclusions

In summary, one contribution of our study is that we demonstrated that small amounts of ethanol admixed to an aqueous solution can regulate the translocation of DNA through polymer-decorated nanopores. We can identify the cononsolvency effect as being responsible for this observation which causes an abrupt collapse of the brush by increasing the alcohol content of the aqueous solution followed by a reswelling at higher alcohol concentration. Regardless of the grafting density of a grafted PNiPAAm polymer layer around the rim of nanopores, in the alcohol-tris buffer mixtures, the polymer layer displays solvent-composition responsive behaviors in the range of metabolic pH values and room temperatures. Our study also shows that a pronounced switching effect can be only realized in a window of moderate grafting densities of PNiPAAm layers. Although in this study PNiPAAm was chosen as a model synthetic polymer, due to the universality of the cononsolvency effect in competitive solvents the conclusions made for PNiPAAm can be extended to other synthetic polymers as well as to biopolymers **[4, 50]**. As a proof of concept of using synthetic polymers to mimic biological functions of cell-membrane channels **[9, 51]**, our study clearly transpired that cononsolvency effect of polymers can be used as a novel trigger **[52]** to change the size of nanopores in analogy to the opening and closure of the gates of cell-membrane channels. We note that achieving any optimization of the concept for some applications it requires a quantitative understanding and characterization of the

cononsolvency response of nanopore brushes which is the main subject of our work.

Another contribution of our study is that using the suction model for the pressure-driven translocation of the DNA chains and on the basis of the DNA-translocation efficiency, for the first time we were able to quantitatively measure effective hydrodynamic thickness of a polymer layer which is grafted around the rim of nanopores. We envisage that our study will spawn further developments for the design of switchable nano-gates and nanopores which are also based on other stimulus-responsive effects such as thermal and pH responses.

ASSOCIATED CONTENT

Supporting Materials

The details of methods used in this study: (1) the method of preparing PNiPAAm-grafted gold membranes; (2) the method of identification and counting of DNA translocation events and the Python source code to realize this method, the method of processing data, information of how to deal with Video Supporting Materials; (3) how to estimate grafting density and morphological regime of polymer brushes. And (i) additional results of DNA translocation experiments for nanopores; (ii) additional results of switch effect of PNiPAAm polymer layers on flat surface both in the ethanol/water mixture and in the ethanol/tris-buffer mixtures. (PDF)

AUTHOR INFORMATION

Corresponding Authors

*yong@ipfdd.de (H.Y.)

*fabien.montel@ens-lyon.fr (F.M.)

*sommer@ipfdd.de (J.-U.S.)

Author Contributions

Huaisong Yong prepared the manuscript draft. Huaisong Yong and Bastien Molcrette conducted the experiments. Marcel Sperling and Huaisong Yong developed the source code to analyze data of DNA translocation experiments. Fabien Montel and Jens-Uwe Sommer directed this work. The manuscript was written through contributions of all authors.

Notes

The authors declare no conflict of finance interest.

ACKNOWLEDGMENTS

This work was supported by the Deutsche Forschungs Gemeinschaft (DFG) under Grant No. SO 277/17. The authors thank Yixuan Du for experiments of scanning electron microscope, and the authors thank Holger Merlitz and Jingguo Li for critical reading the manuscript. The authors also thank Andreas Fery for valuable discussions.

References and Notes

[1] P. Theato, B.S. Sumerlin, R.K. O'Reilly, T.H. Epps, III, Stimuli responsive materials, Chemical Society Reviews, 42 (2013) 7055-7056.

[2] S. Saha, C.A. Weber, M. Nousch, O. Adame-Arana, C. Hoege, M.Y. Hein, E. Osborne-Nishimura, J. Mahamid, M. Jahnel, L. Jawerth, A. Pozniakovski, C.R. Eckmann, F. Julicher, A.A. Hyman, Polar Positioning of Phase-Separated Liquid Compartments in Cells Regulated by an mRNA Competition Mechanism, Cell, 166 (2016) 1572-1584 e1516.

[3] J. Berry, C.P. Brangwynne, M. Haataja, Physical principles of intracellular organization via active and passive phase transitions, Reports on Progress in Physics, 81 (2018) 046601.

[4] O. Matsarskaia, F. Roosen-Runge, F. Schreiber, Multivalent ions and biomolecules: Attempting a comprehensive perspective, Chemphyschem, 21 (2020) 1742-1767.

[5] G. Zhang, C. Wu, The Water/Methanol Complexation Induced Reentrant Coil-to-Globule-to-Coil Transition of Individual Homopolymer Chains in Extremely Dilute Solution, Journal of the American Chemical Society, 123 (2001) 1376-1380.

[6] H.G. Schild, M. Muthukumar, D.A. Tirrell, Cononsolvency in mixed aqueous solutions of poly (N-isopropylacrylamide), Macromolecules, 24 (1991) 948-952.

[7] J.-U. Sommer, Adsorption–Attraction Model for Co-Nonsolvency in Polymer Brushes, Macromolecules, 50 (2017) 2219-2228.

[8] H. Yong, E. Bittrich, P. Uhlmann, A. Fery, J.-U. Sommer, Co-Nonsolvency Transition of Poly(N-isopropylacrylamide) Brushes in a Series of Binary Mixtures, Macromolecules, 52 (2019) 6285-6293.

[9] R.D. Coalson, A.E. Nasrabad, D. Jasnow, A. Zilman, A Polymer-Brush-Based Nanovalve Controlled by Nanoparticle Additives: Design Principles, The Journal of Physical Chemistry B, 119 (2015) 11858-11866.

[10] A.E. Nasrabad, D. Jasnow, A. Zilman, R.D. Coalson, Precise control of polymer coated nanopores by nanoparticle additives: Insights from computational modeling, The Journal of Chemical Physics, 145 (2016) 064901.

[11] C.-W. Li, H. Merlitz, C.-X. Wu, J.-U. Sommer, Nanopores as Switchable Gates for Nanoparticles: A Molecular Dynamics Study, Macromolecules, 51 (2018) 6238-6247.

[12] G. Perez-Mitta, M.E. Toimil-Molares, C. Trautmann, W.A. Marmisolle, O. Azzaroni, Molecular Design of Solid-State Nanopores: Fundamental Concepts and Applications, Advanced Materials, 31 (2019) e1901483.

[13] R. Brilmayer, C. Forster, L. Zhao, A. Andrieu-Brunsen, Recent trends in nanopore polymer functionalization, Current Opinion in Biotechnology, 63 (2020) 200-209.

[14] T. Ma, J.M. Janot, S. Balme, Track-Etched Nanopore/Membrane: From Fundamental to Applications, Small Methods, 4 (2020) 2000366.

[15] Y.A. Perez Sirkin, M. Tagliazucchi, I. Szleifer, Transport in nanopores and nanochannels: some fundamental challenges and nature-inspired solutions, Materials Today Advances, 5

(2020) 100047.

[16] G.W. de Groot, M.G. Santonicola, K. Sugihara, T. Zambelli, E. Reimhult, J. Voros, G.J. Vancso, Switching transport through nanopores with pH-responsive polymer brushes for controlled ion permeability, ACS Applied Materials & Interfaces, 5 (2013) 1400-1407.

[17] G. Emilsson, Y. Sakiyama, B. Malekian, K. Xiong, Z. Adali-Kaya, R.Y.H. Lim, A.B. Dahlin, Gating Protein Transport in Solid State Nanopores by Single Molecule Recognition, ACS Central Science, 4 (2018) 1007-1014.

[18] G. Emilsson, K. Xiong, Y. Sakiyama, B. Malekian, V. Ahlberg Gagner, R.L. Schoch, R.Y.H. Lim, A.B. Dahlin, Polymer brushes in solid-state nanopores form an impenetrable entropic barrier for proteins, Nanoscale, 10 (2018) 4663-4669.

[19] B. Shen, P. Piskunen, S. Nummelin, Q. Liu, M.A. Kostiainen, V. Linko, Advanced DNA Nanopore Technologies, ACS Applied Bio Materials, 3 (2020) 5606-5619.

[20] Z. Zhu, D. Wang, Y. Tian, L. Jiang, Ion/Molecule Transportation in Nanopores and Nanochannels: From Critical Principles to Diverse Functions, Journal of the American Chemical Society, 141 (2019) 8658-8669.

[21] Y.L. Ying, Y.T. Long, Nanopore-Based Single-Biomolecule Interfaces: From Information to Knowledge, Journal of the American Chemical Society, 141 (2019) 15720-15729.

[22] S.M. Lu, Y.Y. Peng, Y.L. Ying, Y.T. Long, Electrochemical Sensing at a Confined Space, Analytical Chemistry, 92 (2020) 5621-5644.

[23] Z.L. Hu, M.Z. Huo, Y.L. Ying, Y.T. Long, Biological Nanopore Approach for Single-Molecule Protein Sequencing, Angewandte Chemie International Edition, DOI 10.1002/anie.202013462(2020).

[24] B. Cressiot, L. Bacri, J. Pelta, The Promise of Nanopore Technology: Advances in the Discrimination of Protein Sequences and Chemical Modifications, Small Methods, 4 (2020) 2000090.

[25] A. Asandei, G. Di Muccio, I. Schiopu, L. Mereuta, I.S. Dragomir, M. Chinappi, T. Luchian, Nanopore-Based Protein Sequencing Using Biopores: Current Achievements and Open Challenges, Small Methods, 4 (2020) 1900595.

[26] W. Shi, A.K. Friedman, L.A. Baker, Nanopore Sensing, Analytical Chemistry, 89 (2017) 157-188.

[27] S. Howorka, Z. Siwy, Nanopore analytics: sensing of single molecules, Chemical Society Reviews, 38 (2009) 2360-2384.

[28] T. Auger, J. Mathe, V. Viasnoff, G. Charron, J.M. Di Meglio, L. Auvray, F. Montel, Zero-mode waveguide detection of flow-driven DNA translocation through nanopores, Physical Review Letters, 113 (2014) 028302.

[29] F. Brochard, P.G. de Gennes, Dynamics of confined polymer chains, The Journal of Chemical Physics, 67 (1977) 52-56.

[30] P.-G. de Gennes, Scaling Concepts in Polymer Physics, Cornell University Press, Ithaca,

NY, USA, 1979.

[31] T. Zheng, M. Zhu, J. Yang, J. He, M. Waqas, L. Li, Revisiting the Flow-Driven Translocation of Flexible Linear Chains through Cylindrical Nanopores: Is the Critical Flow Rate Really Independent of the Chain Length?, Macromolecules, 51 (2018) 9333-9343.

[32] P. Rowghanian, A.Y. Grosberg, Electrophoretic capture of a DNA chain into a nanopore, Physical Review E, 87 (2013) 042722.

[33] A.Y. Grosberg, A.R. Khokhlov, Statistical Physics of Macromolecules, American Institute of Physics, New York, USA, 1994.

[34] P. Hänggi, P. Talkner, M. Borkovec, Reaction-rate theory: fifty years after Kramers, Reviews of Modern Physics, 62 (1990) 251-341.

[35] H.A. Kramers, Brownian motion in a field of force and the diffusion model of chemical reactions, Physica, 7 (1940) 284-304.

[36] P. Huber, Soft matter in hard confinement: phase transition thermodynamics, structure, texture, diffusion and flow in nanoporous media, Journal of Physics: Condensed Matter, 27 (2015) 103102.

[37] G. Bucci, A.J. Spakowitz, Systematic Approach toward Accurate and Efficient DNA Sequencing via Nanoconfinement, ACS Macro Letters, 9 (2020) 1184-1191.

[38] T. Auger, E. Bourhis, J. Donnez, A. Durnez, J.M. Di Meglio, L. Auvray, F. Montel, J. Yates, J. Gierak, Zero-mode waveguide detection of DNA translocation through FIB-organised arrays of engineered nanopores, Microelectronic Engineering, 187-188 (2018) 90-94.

[39] N.A. Bell, M. Muthukumar, U.F. Keyser, Translocation frequency of double-stranded DNA through a solid-state nanopore, Physical Review E, 93 (2016) 022401.

[40] M. Wanunu, W. Morrison, Y. Rabin, A.Y. Grosberg, A. Meller, Electrostatic focusing of unlabelled DNA into nanoscale pores using a salt gradient, Nature Nanotechnology, 5 (2010) 160-165.

[41] Q. Chen, J. Liu, A.E.P. Schibel, H.S. White, C. Wu, Translocation Dynamics of Poly(styrenesulfonic acid) through an α-Hemolysin Protein Nanopore, Macromolecules, 43 (2010) 10594-10599.

[42] A.G. Oukhaled, A.L. Biance, J. Pelta, L. Auvray, L. Bacri, Transport of long neutral polymers in the semidilute regime through a protein nanopore, Physical Review Letters, 108 (2012) 088104.

[43] H. Yong, H. Merlitz, A. Fery, J.-U. Sommer, Polymer Brushes and Gels in Competing Solvents: The Role of Different Interactions and Quantitative Predictions for Poly(N-isopropylacrylamide) in Alcohol–Water Mixtures, Macromolecules, 53 (2020) 2323-2335.

[44] K. Gao, L.T. Kearney, J.A. Howarter, Planar Phase Separation of Weak Polyelectrolyte Brushes in Poor Solvent, Journal of Polymer Science Part B: Polymer Physics, 55 (2017) 370-377.

[45] G. Park, Y. Jung, Many-chain effects on the co-nonsolvency of polymer brushes in a good

solvent mixture, Soft Matter, 15 (2019) 7968-7980.
[46] C. Jentzsch, J.U. Sommer, Polymer brushes in explicit poor solvents studied using a new variant of the bond fluctuation model, The Journal of Chemical Physics, 141 (2014) 104908.
[47] B.C. Choi, S. Choi, D.E. Leckband, Poly(N-isopropyl acrylamide) brush topography: dependence on grafting conditions and temperature, Langmuir, 29 (2013) 5841-5850.
[48] H. Yong, S. Rauch, K.J. Eichhorn, P. Uhlmann, A. Fery, J.U. Sommer, Cononsolvency Transition of Polymer Brushes: A Combined Experimental and Theoretical Study, Materials (Basel), 11 (2018).
[49] J.-U. Sommer, Gluonic and Regulatory Solvents: A Paradigm for Tunable Phase Segregation in Polymers, Macromolecules, 51 (2018) 3066-3074.
[50] C.E. Mills, E. Ding, B.D. Olsen, Cononsolvency of Elastin-like Polypeptides in Water/Alcohol Solutions, Biomacromolecules, 20 (2019) 2167-2173.
[51] R.J. Gilbert, M. Dalla Serra, C.J. Froelich, M.I. Wallace, G. Anderluh, Membrane pore formation at protein-lipid interfaces, Trends in Biochemical Sciences, 39 (2014) 510-516.
[52] W.H. Binder, Polymer-induced transient pores in lipid membranes, Angewandte Chemie International Edition, 47 (2008) 3092-3095.

Supporting Materials: Regulating the translocation of DNA through poly(N-isopropylacrylamide) decorated switchable nanopores by cononsolvency effect

Huaisong Yong[1,2,*], Bastien Molcrette[3], Marcel Sperling[4], Fabien Montel[3,*], and Jens-Uwe Sommer[1,5,*]

[1]Leibniz-Institut für Polymerforschung Dresden e.V., Dresden, Germany

[2]Technische Universität Dresden, Faculty of Chemistry and Food Chemistry, Dresden, Germany

[3] Université de Lyon, École Normale Supérieure de Lyon, Université Claude Bernard, CNRS, Laboratoire de Physique, F-69342, Lyon, France

[4]Fraunhofer-Institut für Angewandte Polymerforschung, Potsdam-Golm, Germany

[5]Technische Universität Dresden, Institute for Theoretical Physics, Dresden, Germany

[*]Correspondence: yong@ipfdd.de (H.Y.); fabien.montel@ens-lyon.fr (F.M.); sommer@ipfdd.de (J.-U.S.)

Contents

S1. Methods

S1.1. Preparation of polymer-grafted gold membrane

The polymer-grafted gold membrane is prepared by following the grafting-to synthetic procedure: (i) The one-side gold-coated membrane (size is about $20mm \times 20mm$) is cleaned with hydrochloric acid (HCl, ≤1.0 mol/L) for an hour at room temperature, then it is cleaned and rinsed in deionized water. (ii) About 4 ml of 10 mg/ml (40mg) α-thiol ω-carboxylic acid terminated poly(N-isopropyl acrylamide) (PNiPAAm, see **Scheme S1**; Polymer Source products were used as received; molecular weight: $M_n = 1.5 \times 10^4\ g/mol$, $M_w/M_n = 1.18$; and $M_n = 3.0 \times 10^4\ g/mol$, $M_w/M_n = 1.25$; for detail please refer TDS files from Polymer Source) in deionized water is reduced with 0.1 mmol (30mg) tris(2-carboxyethyl)phosphine hydrochloride (TCEP, Sigma-Aldrich products were used as received). Then the polymer solution is filtered by using 200nm-size PEFE filter. (iii) The cleaned gold membrane is immersed in the filtered PNiPAAm solution and incubated 24-96 hours; the reaction temperature is close to but lower than the LCST transition temperature of PNiPAAm (about 32°C), in this study the reaction temperature is 30 °C. (iv) After grafting reaction, to remove the non-reacted PNiPAAm and TCEP, the polymer-grafted gold membrane is immersed in deionized water reservoir at least 4 hours.

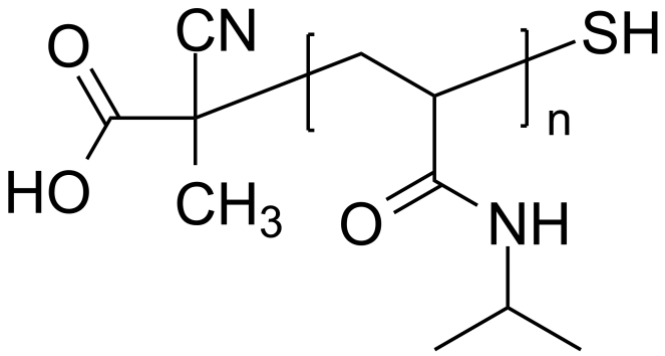

Scheme S1. The molecular structure of α-thiol ω-carboxylic acid terminated poly(N-isopropyl acrylamide) that used in our grafting reactions. Information is provided by the TDS (technical data sheets) files of Polymer Source products.

In the above protocol, we used the grafting-to synthetic method to prepare polymer-grafted membrane. The advantage of this approach is that the molecular weight and its distribution of a polymer layer can be well approximated to its free polymer in solutions **[1]** in advance in contrast to grafting-from method, this is exact the case in our study when the polydispersity of polymer in solutions is narrow (close to 1.0), see **Table S1**. However, it is still impossible to measure the thickness of the polymer layer around the rim of nanopores by using current-known analytical methods. In this study, this problem is overcome based on a suction model

[2-4] with helps of translocation dynamics of fluorescence DNA, see **section 2.2** of **main text**. This allows us to estimate the grafting densities and the morphological regimes of polymers that grafted around the rim of nanopores.

Nevertheless, it is necessary to properly design experiments to cross verify analysis based on our measurement techniques. To qualitatively know grafting-density difference between two batch of grafted polymers, as for the lower-molecular-weight samples ($M_n = 1.5 \times 10^4$ *g/mol*, M_w/M_n = 1.18), first we used the fresh PNiPAAm solution to prepare higher grafting-density polymer and the grafting reaction time was 96 hours, then we re-used the "reacted" or "waste" PNiPAAm solution to prepare lower grafting-density polymer and the grafting reaction time was 48 hours. The methodology behind this approach is that: polymer materials always have a molecular weight distribution. Because of the polymer chain's huge size relative to its end functional groups and steric hindrance in the grafting reaction, shorter polymer chains prefer to react with the gold surface first, then turns to the longer polymer chains. This is also the intrinsic reason why it is hard to get a very high grafting density for polymers with long chains by the method of grafting-to synthetic approach in preparing polymer brushes. Recently this phenomenon was revisited by **ref. [1]**. Our approach is also designed to check the protocol's reliability. As for higher-molecular-weight samples ($M_n = 3.0 \times 10^4$ *g/mol*, M_w/M_n = 1.25), the grafting reaction time for the lower-grafted sample is 24hours, and the grafting reaction time for the higher-grafted sample is 72 hours. The physical parameters of grafting reaction used in this study for higher and lower grafted membranes with different molecular weights, are summarized in **Table S1**.

Table S1. The physical parameters of grafting reaction used in this study for higher and lower grafted membranes with different molecular weights.

sample name	**time of grafting reaction**	**molecular weight** (M_n, ***g/mol***)	**PDI** (solutions)	**reaction temperature**	**solution quality**
higher-graft-15K	96 hours	1.5×10^4	1.18	30 °C	fresh
lower-graft-15K	48 hours	1.5×10^4	1.18	30 °C	reuse*
higher-graft-30K	72 hours	3.0×10^4	1.25	30 °C	fresh
lower-graft-30K	24 hours	3.0×10^4	1.25	30 °C	fresh

*The fresh polymer solution is already used by the sample "higher-graft-15K".

It is worth pointing out that analysis results (**Table 1** of **main text**) based on our analytic method developed in **section 2.2** of **main text**, are consistent with our experimental design in a somewhat intuitive way: the longer the time of grafting reaction and the higher the activity of the reactive solution, the thickness is higher for the grafted polymers when with the same molecular weight.

S1.2. The method of identification and counting of DNA translocation events

We accomplished the counting of DNA translocation events (a kind of moving objects) using a customized algorithm to ensure objectivity as well as high reproducibility of the evaluation results including efficiency regarding their acquisition. The algorithm was implemented by in-house scripts coded in Python v3.7.3 (https://www.python.org) with numpy v1.16.4 (https://numpy.org) and openCV (https://openCV.org] v4.1.1.26).

Firstly, the video files are converted into raw image stacks by software such as ImageJ, which are fed into the program. Each image is then subjected to a noise-background subtraction considering a defined brightness percentage (noise-background strength, in our experiments is about 15%). One problem in our experiments concerns the size of a real flash (a DNA translocation event). It is obvious that a flash may be too small to be a real DNA translocation event. Therefore, a threshold has to be defined to ignore too small closed contours (artefact DNA translocation events); this threshold is about a 5x5 pixel matrix in images in our video data. Then, images are processed by image blurring using a blur matrix, the blurring threshold is about a 18x18 pixel matrix for the blur matrix in our video data, note that the mean-blur method is used in this study. The blurring is used to reduce interrupted object contours, which are determined next by a simple binary threshold routine. The contours are characterized by their center of mass, i.e., location within the image and size. This routine is repeated for all frame images unpacked from the video, thereby completing the time stack for each experiment. It is worth pointing out that artifacts arising from small but true objects are prevented by a minimum-size blurring threshold for the contours to be accepted.

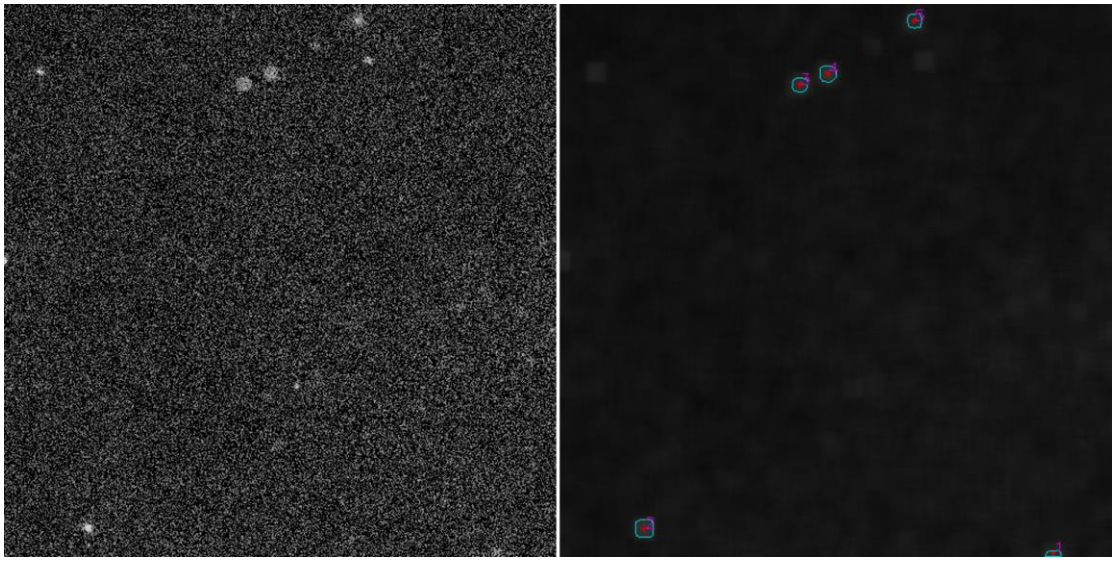

Figure S1. An example to determine the number of DNA translocation events for the blank membrane (without grafting PNiPAAm polymer) under the driving pressure of 35 mbar and in tris buffer solutions (without ethanol). The left picture is the first frame of an original video data and the right picture is the counting results for the left picture. Note that the vision size of video data (one frame) is fixed in an area of $A = 135\mu m \times 135\mu m$.

One major problem in our experiments concerning the automatic identification of valid DNA translocation events, was the prolonged duration of single events exceeding that of one video frame. Accordingly, simple counting of contours in each single image will result in a significant over estimation of events. We therefore introduced another threshold parameter, namely the travel distance. Based on the individual flash size (a DNA translocation event), the travel distance value determines the distance, by which a DNA translocation is allowed to be displaced between consecutive image frames. Binding this value proportionally to the flash size seemed reasonable to us, since for bigger flashes, the inherent fluctuation with respect to the determination of its center of mass for two consecutive frame images might be somewhat higher than for smaller flashes. Thus, we could successfully prevent an overcounting of DNA translocation events by only counting the objects that were sufficiently separated in terms of their location within consecutive frames and correctly identifying DNA translocation events lasting for several frames.

Noise-background strength could be quite different for different video data. To estimate the noise-background strength of each video as objectively as possible, firstly the smaller number of DNA translocation events (less than 250 in this study) of videos is accurately counted by human eyes, because it is very hard for human eyes to focus on and accurately count larger number of DNA translocation events. Then the Python code is used to estimate noise-background strength of these videos to make sure the counting results of Python code are as close as possible to the counting results of human eyes. Finally, the average noise-background strength of these videos is used to count the same batch experiments of videos which contain a larger number of DNA translocation events (more than 250 in this study). It is expected that this approach is reasonable since for the same batch of experiments, only an experimental parameter of pressure is changed in the experiments and the contrast of each video is already adjusted at the same level and as clearly as possible for the same batch of experiments.

Figure S1 is an example to determine the number of DNA translocation events based on the algorithm applied in this study. This result is obtained by the following procedure: (i) Open the video in ImageJ (https://imagej.net/Fiji), subtract instrument background. (ii) The video files are converted into raw image stacks with 32-bit depth by ImageJ. (iii) The raw image stacks are fed into the program. Set noise-background subtraction for images, in this study it is 15%. Set a threshold that excludes an artefact DNA translocation event, this threshold is about a 5x5 pixel matrix in images in our video data. Set blur matrix for images, in this study the blurring threshold is about a 18x18 pixel matrix. Set the travel distance for DNA translocation events, in this study it is about 3 times of flash size. The program also needs to know the bit-depth of raw image stacks, this value of depth shall be the same as the value of depth generated by ImageJ, in our study it is 32 bits by ImageJ. (iv) Run the program, the counting result will be marked

on the images. A comparison between original and marked translocation events in video data can be found in **Video Supporting Materials**, also see **section S1.3**.

S1.3. Information of how to deal with Video Supporting Materials

Following the same procedure and the same parameter values that are used to process image data of **Figure S1,** see **section S1.2**, the counting results are automatically marked on the videos. The two video samples are from the same batch of experiments for the blank membrane (without grafting PNiPAAm polymer) in tris buffer solutions (without ethanol). The video sample with much more flash events are experimental data that are collected under a higher driving pressure (45 mbar), the video sample with less flash events are experimental data that are collected under a lower driving pressure (35 mbar). If readers patiently count the number of flash events for the **Video Supporting Materials**, the counting results by Python code (175 and 387) will be close to the results counted by human eyes (about 170 and 370), respectively.

S1.4. The method of processing data

The mean value of DNA translocation events (N_{DNA}) is

$$N_{DNA} = \frac{1}{n}\sum_{i}^{n} N_{DNA,i} \ . \tag{S1}$$

The error bar of DNA translocation events (ΔN_{DNA}) in this study is defined as its average absolute deviation instead of popular used standard deviation, because one could not simply assume that the data sample must comply with a "bell-shaped" statistical distribution such as Gaussian distribution **[5]**. The average absolute deviation does not require a data sample to comply with a specific statistical distribution, this is also a necessary choice when the amount of data in a sample is small,

$$\Delta N_{DNA} = \frac{1}{n}\sum_{i=1}^{n} \left| N_{DNA,i} - N_{DNA} \right| . \tag{S2}$$

One can further use **Eq.(S1)**, **Eq.(S2)** and **Eq.(6)** (**main text**) to calculate the translocation frequency of DNA per pore (f_{DNA}) and its error bar (Δf_{DNA}).

The critical pressure (P_c) can be obtained by fitting the nonlinear equation **Eq.(2a)** (**main text**), we rewrite it here,

$$f_{DNA} = k_2 \left(\frac{P}{P_c} \right) \exp(-\frac{P_c}{P}) \ , \tag{S3}$$

where P is the gradient of pressure applied in experiments. In practice, when P_c/P is small, **Eq.(S3)** reduces to a linear equation,

$$f_{DNA} = \frac{k_2}{P_c} P - k_2 \,. \qquad \text{(S4)}$$

Therefore, a linear fit procedure of **Eq.(S4)** is preferable when the data show an asymptotic linear behaviour between the translocation frequency of DNA per pore (f_{DNA}) and the pressure (P), otherwise a nonlinear fit procedure of **Eq.(S3)** is a necessary choice. Note that k_2 (Hz) in **Eq.(S3)** and **Eq.(S4)** is a constant for a given system. The key to get an error bar (ΔP_c) of the critical pressure is to use $f_{DNA} + \Delta f_{DNA}$, $f_{DNA} - \Delta f_{DNA}$ and f_{DNA} to fit **Eq.(S3)** and **Eq.(S4)**. **Figure S2** and **Figure S3** are examples of determining an error bar of a critical pressure by using **Eq.(S3)** and **Eq.(S4)**, respectively.

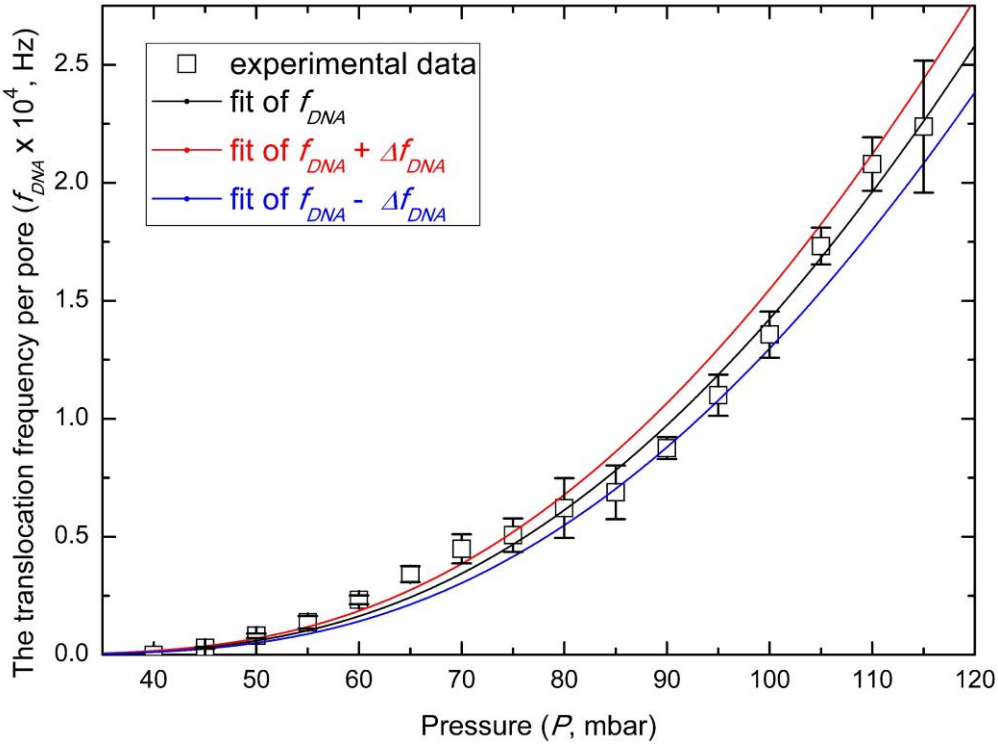

Figure S2. A graphic description how to get an error bar (ΔP_c) of a critical pressure by using **Eq.(S3)**.

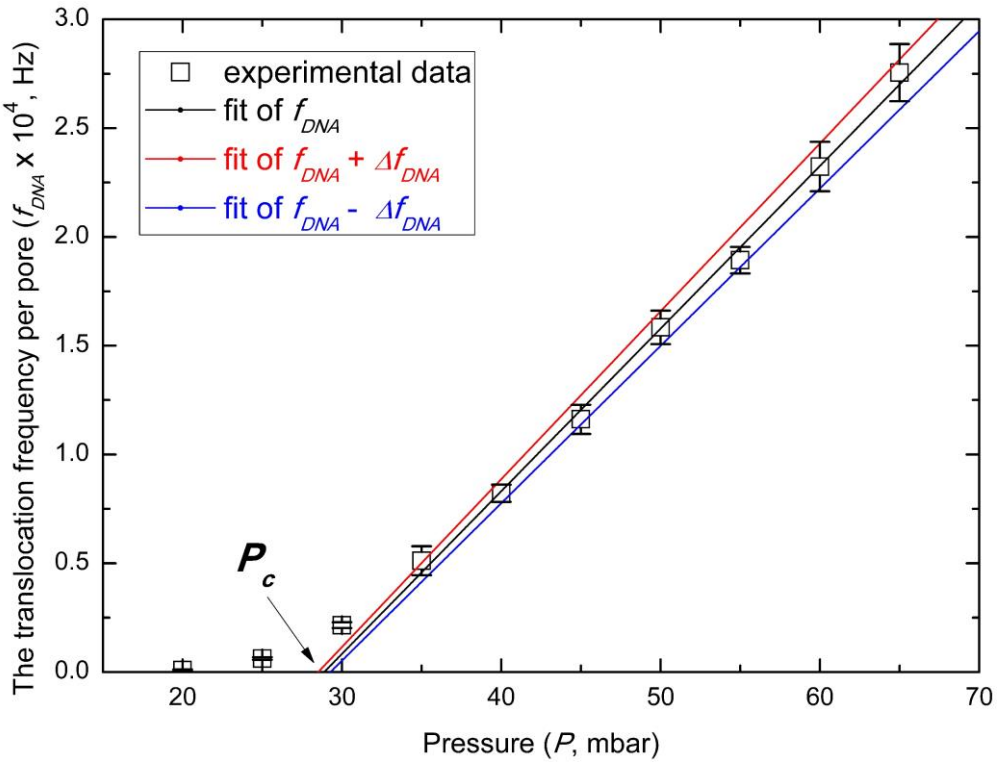

Figure S3. A graphic description how to get an error bar (ΔP_c) of a critical pressure by using **Eq.(S4)**.

S1.5. An estimation of grafting density and morphological regime

From the determined film thickness (h) in the dry state, polymer brush parameters like grafting density (σ) and distance between anchoring points (S) can be calculated by using the simple relation:

$$\sigma = \frac{1}{S^2} = \frac{N_A \rho h}{M_n}, \tag{S5}$$

where M_n is the number-average molecular weight of the polymer, N_A is the Avogadro's constant, ρ is the polymer's melt density. Here, ρ is 1.1 g/cm^3 for PNiPAAm homo-polymer. For the interpretation of our measurements, we have to assume a lateral homogeneous polymer profile in the dry state. This is the case for the brush regime of strongly overlapping chains. To determine whether the grafted polymers are in the brush regime, the distance between grafting sites, S, should be small enough. For the case of a good solvent, S should be much smaller than twice the radius of gyration of the chains (R_G):

$$\frac{S}{2} < R_G = \alpha N^{0.588}, \tag{S6}$$

where α is a prefactor proportional to the monomer size and N is the degree of polymerization; for the PNiPAAm polymer, α is estimated to be 0.25 nm. However, in the collapsed state, this

condition is not sufficient. Here, so-called octopus-micelles **[6, 7]** can be formed if the grafting density is below the stretching threshold of σ^{**},

$$\sigma^{**} = \frac{N_A \rho \alpha}{M_0 \sqrt{N}}, \tag{S7}$$

where M_0 is the molecular weight of repeat units of the polymer. If $\sigma > \sigma^{**}$, the chains will form stretched brushes. This condition gives an estimation for the grafting density, which is necessary for a homogeneous brush in the collapsed state. One might also use the overlap radius of gyration of the chains (R_P) between collapsed single chains as a rough lower estimate for a homogeneous brush under the condition that chains collapse mostly, i.e., $R_P = \alpha N^{1/3}$ and $S/2 < R_P$, where the radius of gyration under poor solvent conditions is taken. We note that this estimation slightly underestimates the necessary grafting density.

As for a grafted polymer layer, if it is in the brush regime, the following relation shall hold:

$$\begin{aligned} H &\approx \frac{N}{g} D_{blob}, \\ D_{blob} &\approx \alpha g^{\nu} \end{aligned} \tag{S8}$$

where H is the swollen thickness of polymer layer, D_{blob} is the thermal blob size, g is the number of monomers in a thermal blob, and $\nu = 0.588$ is the Flory exponent for a polymer chain in a good solvent. It is also noted that

$$D_{blob} \approx S = \frac{1}{\sqrt{\sigma}}. \tag{S9}$$

Substitute **Eq.(S9)** into **Eq.(S8)**, we get

$$\sigma \approx \left(\frac{H}{N \alpha^{\frac{1}{\nu}}} \right)^{\frac{2\nu}{1-\nu}}. \tag{S10}$$

Here, it is worth pointing out that **Eq.(S10)** can be approximately used to determine a polymer brush's grafting density if we cannot directly measure thickness of a dry polymer layer, see **Eq.(S5)**. It is also noted that under strong flow pressure, the polymer layer is compressed and that **Eq.(S5)** can be approximately used to determine the upper boundary of grafting density; for this case, the maximum grafting density is estimated with replacing the dry thickness (h) by the compact swollen thickness ($H_{collapse}$) as

$$\sigma_{\max} < \frac{N_A \rho H_{collapse}}{M_n}. \tag{S11}$$

In this study, the error bar for the normalized swollen thickness of polymer layer $\Delta(H/H_0)$ is estimated by the following equation,

$$\Delta\left(\frac{H}{H_0}\right) = \sqrt{\frac{\left(\Delta H\right)^2}{H_0^2} + \frac{H^2}{H_0^4}\left(\Delta H_0\right)^2}, \tag{S12}$$

which is a Taylor expansion for the propagation of uncertainty, note that in this equation we implicitly assume H and H_0 are independent with each other because these two variables are measured in different and independent experiments. Here, the reference value (H_0) for normalization in this study is the swollen thickness of the polymer layer in pure water or tris buffer solutions (without ethanol). In this study, we also use this definition for the error bar of the normalized translocation frequency of DNA per pore ($f_{DNA}/f_{DNA,\ 0}$) where $f_{DNA,\ 0}$ is the translocation frequency of DNA per pore observed in tris buffer solutions (without ethanol).

S2. Additional results of DNA translocation experiments for nanopores

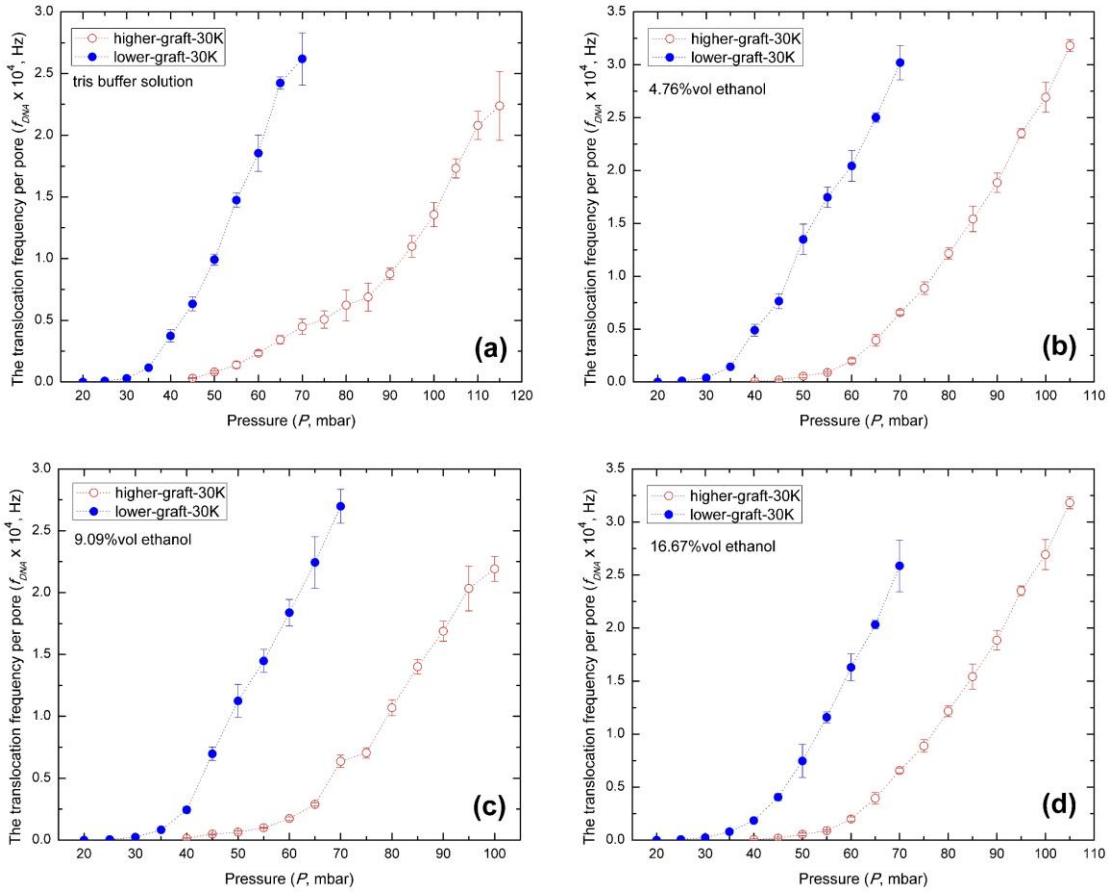

Figure S4. The translocation frequency of DNA per pore with respect to pressure when DNAs translocate through nanopores with different polymer grafting densities: (a) in tris buffer solutions, (b) in 4.76%vol ethanol-tris buffer mixtures, (c) in 9.09%vol ethanol-tris buffer mixtures, (d) in 16.67%vol ethanol-tris buffer mixtures.

As for PNiPAAm-grafted nanopores, the molecular weight of the PNiPAAm polymer is M_n = 3.0 x 10^4 *g/mol*, M_w/M_n = 1.25. The size of blank nanopores is 50 nm. pH value of the buffer is about 7.6 and the test temperature is 298 K. The dotted lines in the figures are guides to eyes.

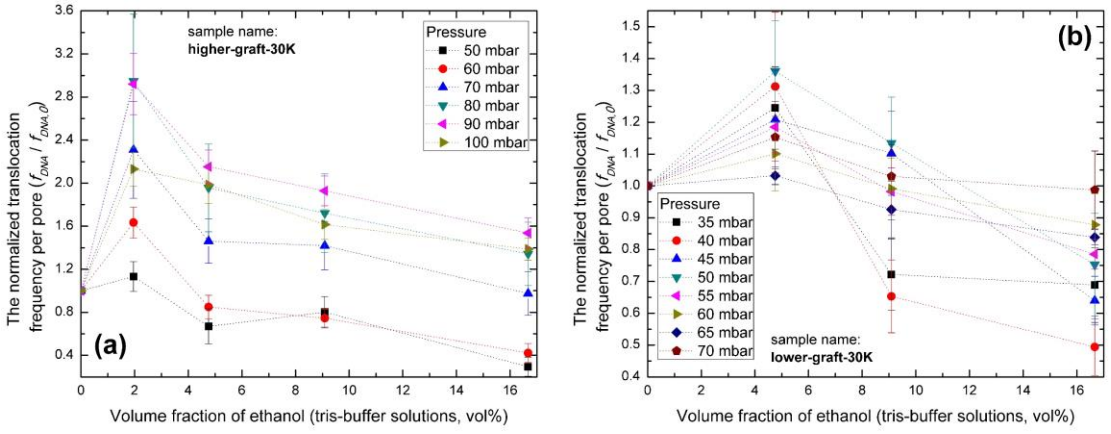

Figure S5. The normalized translocation frequency of DNA per pore is plotted with respect to ethanol

concentration change under different driving pressure. (a) For the higher grafting densities of PNiPAAm-grafted nanopores, data are already used in **Figure 5a** (**main text**). (b) For the lower grafting density of PNiPAAm-grafted nanopores, data are already used in **Figure 5b** (**main text**). Note that $f_{DNA,\,0}$ is the observed translocation frequency of DNA per pore in tris buffer solutions (no addition of ethanol). Molecular weight of the PNiPAAm polymer is $M_n = 3.0 \times 10^4\ g/mol$, $M_w/M_n = 1.25$. The size of blank nanopores is 50 nm. pH value of the buffer is about 7.6 and the test temperature is 298 K. The dotted lines in the figures are guides to eyes.

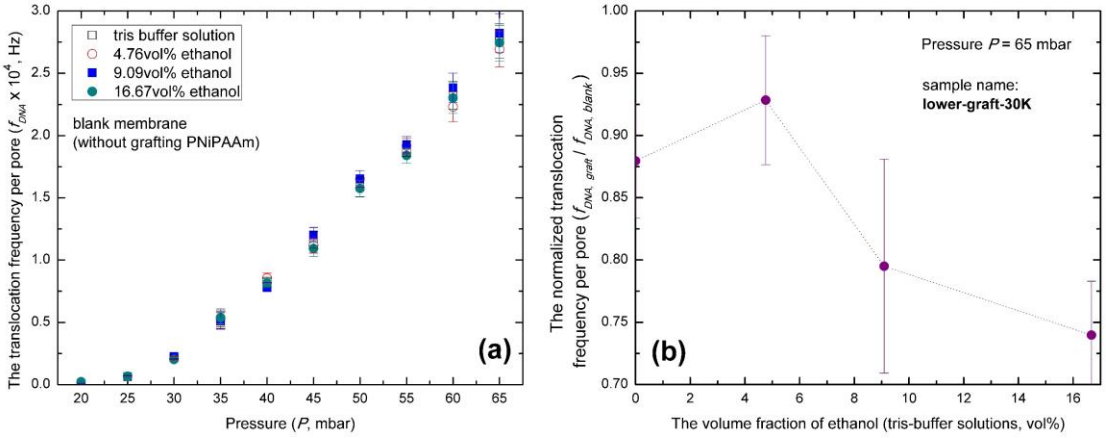

Figure S6. Control experiments for blank membrane without grafting a PNiPAAm layer in various mixtures of ethanol and tris buffer. (a) The translocation frequency of DNA per pore with respect to pressure. (b) The normalized translocation frequency of DNA per pore is plotted with respect to ethanol concentration when the driving pressure P is 65 mbar. Note that $f_{DNA,\,graft}$ is the observed translocation frequency of DNA per pore for the sample "lower-graft-30K" with a very low grafting density, and $f_{DNA,\,blank}$ is the observed translocation frequency per pore for the blank membrane. pH value of the buffer is about 7.6 and measurement temperature is at 25 °C.

S3. Switch effect of polymer layers on flat surface

S3.1. Grafting-density effect of flat PNiPAAm layers in ethanol/water mixtures

Although our DNA translocation experiments clearly indicated that the grafted PNiPPAm polymers around the rim of nanopores show signatures of re-entrant and switchable effect with respect to ethanol concentration, it is not clear whether these signatures are true equilibrium behaviors, since our DNA translocation experiment is a kind of somewhat quasi-equilibrium method **[2, 4]**. Actually, under certain situations, few experiments reported that cononsolvency of poly(N-n-propylacrylamide) **[8]** and PNiPAAm **[9]** show non-equilibrium phase-transition behaviors in the alcohol/water mixtures. To further check our observations in DNA translocation experiments, we used in-situ Vis-spectroscopic ellipsometry method to study equilibrium swollen thickness of flat PNiPAAm layers both in ethanol-water mixtures and ethanol/tris buffer mixtures. The details of conducting ellipsometry experiments were already reported in our previous studies, for details please refer to **ref.[10]**.

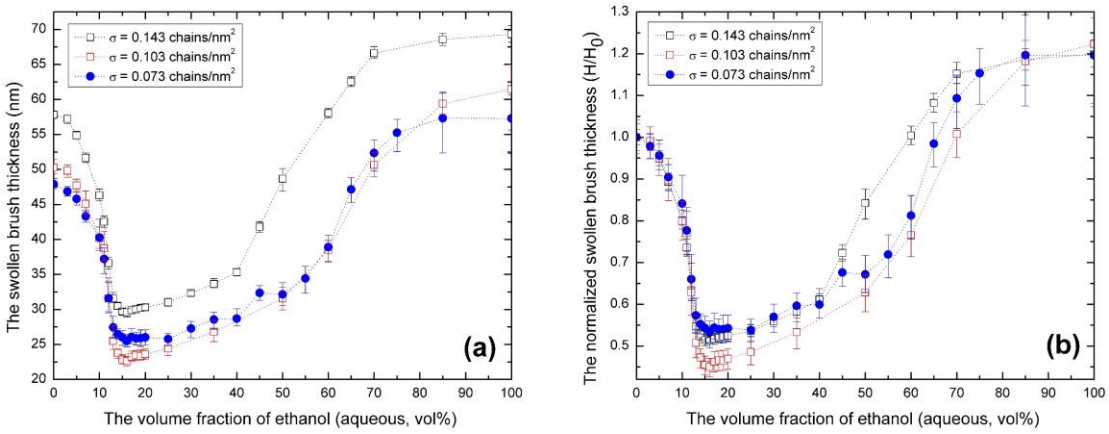

Figure S7. A study of in-situ Vis-spectroscopic ellipsometry for equilibrium swollen polymer thickness on grafting-density effect in the cononsolvency transition of grafted PNiPAAm polymers in ethanol/water mixtures on the flat surface, at the temperature of 25°C: (a) absolute swollen polymer thickness; (b) normalized swollen polymer thickness. Experiments were conducted in ethanol aqueous solutions with the molecular weight of M_n = 6.1×10^4 g/mol, M_w/M_n = 1.40 for all polymer layers. The dotted lines in the figures are guides to eyes.

Figure S7 shows measurements of in-situ Vis-spectroscopic ellipsometry for equilibrium swollen thickness of grafted PNiPAAm in ethanol/water mixtures on flat surface. The data for the absolute brush thickness as a function of the volume fraction of ethanol are displayed in **Figure S7a** (some data were already reported in our previous study **[11]**). The absolute swollen brush thickness at the collapse state clearly showed that when the brush layer's grafting density (σ) is lower than a threshold grafting density (σ^{**}, how to determine this threshold see **Eq.(S7)**), the collapsed polymer layer (blue filled-circles in **Figure S7a**) is thicker than a brush layer (red open-square in **Figure S7a**) whose grafting density is higher than the threshold grafting density. In **Figure S7b**, we again display the normalized swollen brush thickness for the same systems as shown in **Figure S7a**. From **Figure S7**, it shows that when the grafting density (σ) reaches a critical threshold (σ^{**}) for a polymer layer, a decrease of grafting density weakens the collapse, this is quite different from phase behaviors of a classic polymer brush for which the brush thickness (H) is proportional to grafting density (σ) at the poor-solvent state. It indicates that the polymer layer which has the lowest grafting density (blue filled-circles in **Figure S7**), maybe locate in the so-called octopus-shape micelle region. It is noted that computer simulation studies **[12, 13]** on cononsolvency transition of grafted polymer layers have also observed octopus-shape micelle morphologies.

S3.2. Switch effect of PNiPAAm layers on flat surface in ethanol/tris buffer mixtures

We repeated experiments for flat polymer layers (***the same flat polymer layers*** as shown in **Figure S7**) in ethanol/tris buffer mixtures on flat surface, see **Figure S8**. Although in **Figure S8**

water is replaced by the tris buffer, the ellipsometry study clearly indicates that the PNiPAAm layers show collapse behaviors with respect to an increase of ethanol concentration. Like in **Figure S7**, we also observed the same tendency of grafting-density effect for these flat polymer layers in ethanol/tris buffer mixtures, it once again showed that a pronounced switching effect can only be realized in a window of moderate grafting densities. It is also worthy of noting that from the comparison of each grafting density in **Figure S7** and **Figure S8**, it can be seen that the collapse transition is stronger in ethanol/water mixtures than in ethanol/tris buffer mixtures; the reason for this observation may be ascribed to the additional competition adsorptions of tris-buffer compositions (such as EDTA and tris) on PNiPAAm polymer chains, the additional competition adsorptions effectively reduce the competition-adsorption strength between ethanol and polymer chains. Our previous mean-field studies showed that a reduction of competition-adsorption strength between alcohol and PNiPAAm, can lead to a weaker collapse transition in cononsolvency **[11, 14]**. However, this explanation is still speculative, currently the molecular reason behind this observation is still unclear.

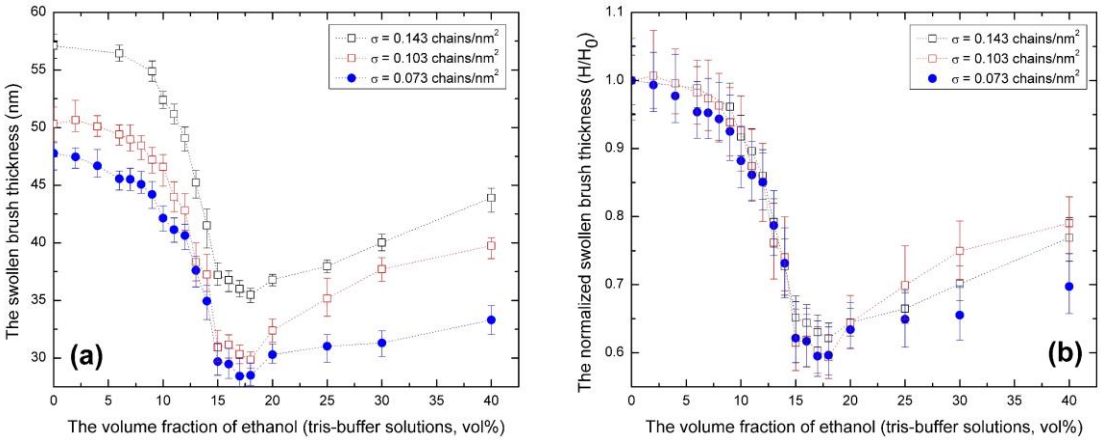

Figure S8. A study of in-situ Vis-spectroscopic ellipsometry for equilibrium swollen polymer thickness on grafting-density effect in the cononsolvency transition of grafted PNiPAAm polymers in ethanol/tris buffer mixtures on the flat surface, at the temperature of 25°C, the pH value of the buffer is 7.45: (a) absolute swollen polymer thickness, (b) normalized swollen polymer thickness. Experiments were conducted in ethanol/tris buffer mixtures with the molecular weight of $M_n = 6.1\times10^4$ g/mol, $M_w/M_n = 1.40$ for all polymer layers. The dotted lines in the figures are guides to eyes.

As an example, **Figure S9** checks the reproducibility of our experimental results for PNiPAAm brushes when the pH value of the tris buffer is 7.45. In the repeating experiments, we used ***the same brush*** for the repeating measurements.

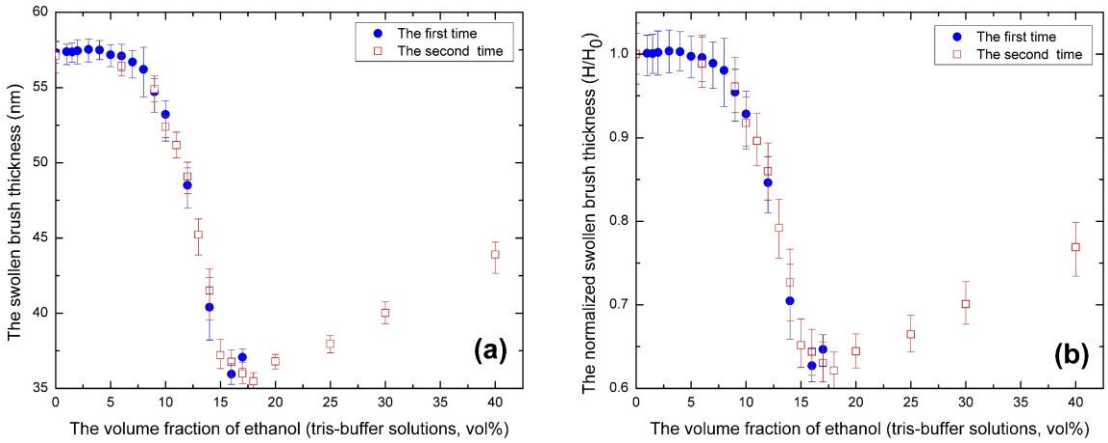

Figure S9. Repeating experiments for swollen brush thickness as a function of ethanol concentration when the pH value of the buffer is 7.45. Parameters of the PNiPAAm brush are grafting density 0.143 *chains*/nm^2, M_n = 6.1 x 10^4 *g/mol*, and M_w/M_n = 1.40. Measurement temperature is at 25 °C.

Typical real-time measurements of in-situ Vis-spectroscopic ellipsometry for swollen flat brush thickness of PNiPAAm in tris buffer/ethanol mixtures are shown in **Figure S10**. Note that it is impossible to do cononsolvency experiments at very high concentration of ethanol when admixed with tris buffer, because the salt compositions in tris buffer will precipitate when the concentration of ethanol is very high.

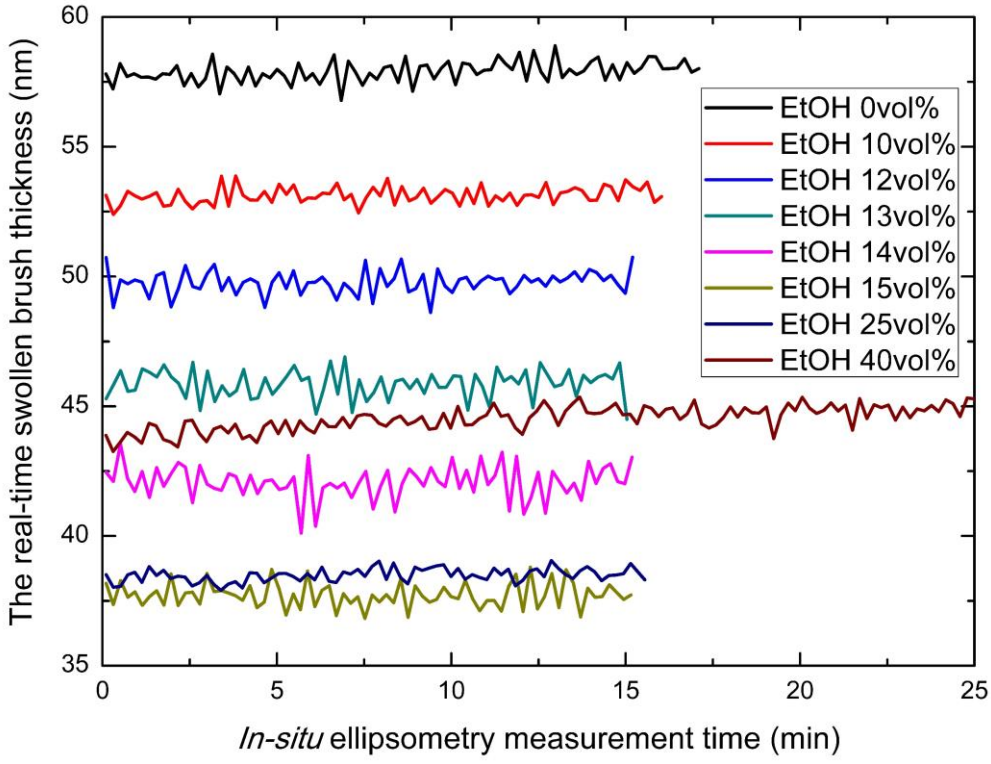

Figure S10. The swollen brush thickness of a PNiPAAm brush on flat surface in ethanol/tris buffer mixtures: the

real-time swollen brush thickness of the PNiPAAm brush as a function of measurement time, the pH value of the buffer is 7.45. Parameters of the PNiPAAm brush are grafting density 0.143 *chains/nm*^{2}, M_n = 6.1 x 10^4 *g/mol*, and M_w/M_n = 1.40. Measurement temperature is at 25 °C.

A summary of the normalized swollen thickness of ***the same flat PNiPAAm brush*** with respect to ethanol concentration at various pH values of the buffer solution is plotted in **Figure S11**. **Figure S11** shows that when the volume fraction of ethanol is less than 15%, the collapse transition, i.e., the left branch of cononsolvency transition becomes stronger with a decreasing of pH value of tris buffer, currently the reason behind this observation is still unclear. As shown in **Figure S11**, when the volume fraction of ethanol is larger than 15%, the situation becomes intricate for the right branch of cononsolvency transition, we cannot get a clear conclusion on the effect of changing pH based upon current experimental data; a detailed study of this topic is beyond the scope of this study and will be investigated in future.

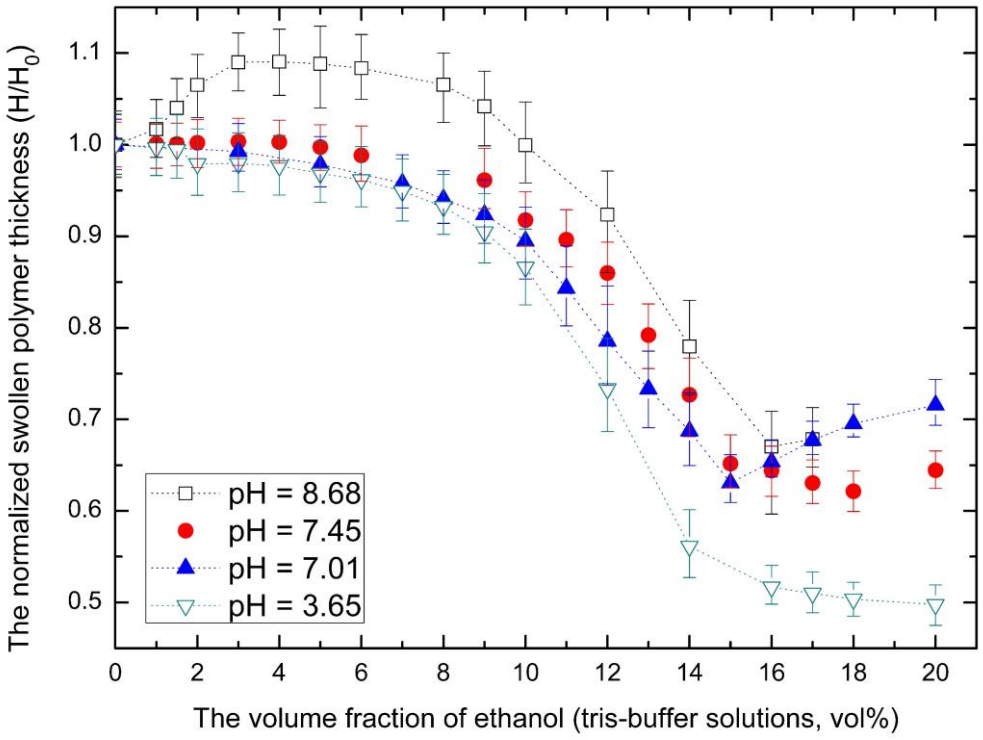

Figure S10. The swollen brush thickness of a PNiPAAm brush on flat surface in ethanol/tris buffer mixtures: the normalized swollen brush thickness as a function of ethanol concentration obtained via in-situ Vis-ellipsometry at different pH values of buffer solutions. Parameters of the PNiPAAm brush are grafting density 0.143 *chains/nm*^{2}, M_n = 6.1 x 10^4 *g/mol*, and M_w/M_n = 1.40. Measurement temperature is at 25 °C.

References and Notes

1. Lukas Michalek, Kai Mundsinger, Christopher Barner-Kowollik, and Leonie Barner. The long and the short of polymer grafting. *Polymer Chemistry*, ***2019***, 10, 54-59.

2. Tao Zheng, Mo Zhu, Jinxian Yang, Jing He, Muhammad Waqas, and Lianwei Li. Revisiting the Flow-Driven Translocation of Flexible Linear Chains through Cylindrical Nanopores: Is the Critical Flow Rate Really Independent of the Chain Length? *Macromolecules*, ***2018***, 51(22), 9333-9343.
3. Thomas Auger, Jérôme Mathé, Virgile Viasnoff, Gaëlle Charron, Jean-Marc Di Meglio, Loïc Auvray, and Fabien Montel. Zero-Mode Waveguide Detection of Flow-Driven DNA Translocation through Nanopores. *Physical Review Letters*, ***2014***, 113, 028302.
4. Pierre-Gilles de Gennes. *Scaling Concepts in Polymer Physics*; Cornell University Press: Ithaca, NY, USA, 1979; ISBN 978-0801412035.
5. Two books have deeply discussed various issues of using standard deviation. (a) Gary Smith. *Standard Deviations: Flawed Assumptions, Tortured Data, and Other Ways to Lie with Statistics* (*1st edition*). Harry N. Abrams, Inc., ***2014***, ISBN-13: 978-1468309201; (b) Nassim Nicholas Taleb. *Statistical Consequences of Fat Tails: Real World Preasymptotics, Epistemology, and Applications*. ***2020***, arXiv:2001.10488.
6. Christoph Jentzsch, and Jens-Uwe Sommer. Polymer brushes in explicit poor solvents studied using a new variant of the bond fluctuation model. *The Journal of Chemical Physics*, ***2014***, 141, 104908.
7. B.-C. Choi, S. Choi, and D. E. Leckband. Poly(N-isopropyl acrylamide) brush topography: dependence on grafting conditions and temperature. *Langmuir*, ***2013***, 29, 5841-5850.
8. Hideya Kawasaki, Takato Nakamura, Keiichi Miyamoto, Masayuki Tokita, and Takashi Komai. Multiple volume phase transition of nonionic thermosensitive gel. *The Journal of Chemical Physics*, 1995, 103, 6241-6247.
9. Na Xue, Xing-Ping Qiu, Vladimir Aseyev, and Francoise M. Winnik. Nonequilibrium Liquid−Liquid Phase Separation of Poly(N-isopropylacrylamide) in Water/Methanol Mixtures. *Macromolecules*, ***2017***, 50(11), 4446-4453.
10. Huaisong Yong, Sebastian Rauch, Klaus-Jochen Eichhorn, Petra Uhlmann, Andreas Fery, and Jens-Uwe Sommer. Co-nonsolvency Transition of Polymer Brushes: A Combined Experimental and Theoretical Study. *Materials*, 2018, 11, 991.
11. Huaisong Yong, Eva Bittrich, Petra Uhlmann, Andreas Fery, and Jens-Uwe Sommer. Co-nonsolvency transition of poly(N-isopropylacrylamide) brushes in a series of binary mixtures. *Macromolecules*, ***2019***, 52, 6285-6293.
12. Andre Galuschko, and Jens-Uwe Sommer. Co-Nonsolvency Response of a Polymer Brush: A Molecular Dynamics Study. *Macromolecules*, ***2019***, 52, 4120-4130.
13. Gyehyun Park, and YounJoon Jung. Many-chain effects on the co-nonsolvency of polymer brushes in a good solvent mixture. *Soft Matter*, ***2019***, 15, 7968-7980.
14. Huaisong Yong, Holger Merlitz, Andreas Fery, and Jens-Uwe Sommer. Polymer Brushes and Gels in Competing Solvents: The Role of Different Interactions and Quantitative Predictions for Poly(N-isopropylacrylamide) in Alcohol–Water Mixtures. *Macromolecules*, ***2020***, 53, 2323-2335.